

SEQUENCE STRATIGRAPHIC ANALYSIS & ANISOTROPIC ELASTIC
MODULI DETERMINATION OF THE VACA MUERTA FORMATION,
NEUQUEN BASIN, ARGENTINA.

by

Paula Andrea Carolina Barbosa Murillo

© Copyright by Paula Andrea Carolina Barbosa Murillo, 2017

All Rights Reserved

A thesis submitted to the Faculty and the Board of Trustees of the Colorado School of Mines in partial fulfillment of the requirements for the degree of Master of Science (Geophysical Engineering).

Golden, Colorado

Date _____

Signed: _____
Paula Andrea Carolina Barbosa Murillo

Signed: _____
Dr. Thomas L. Davis
Thesis Advisor

Golden, Colorado

Date _____

Signed: _____
Dr. Roel Snieder
Professor and Head
Department of Geophysics

ABSTRACT

The Vaca Muerta Formation (VM) is considered the fourth largest shale oil play in the world with an estimated 27 billion barrels of recoverable oil. The VM, as other unconventional reservoirs, contains layers with substantial velocity anisotropy. Former studies performed an isotropic characterization of the VM. Fernandez-Concheso M. (2015) worked on post and pre-stack seismic inversions to supply a tool to characterize the VM. Bishop (2015) developed a mechanical stratigraphy for the VM to evaluate its influence in the success of stimulation jobs. This study involves sequence stratigraphic analysis as a basis for estimating anisotropic elastic moduli, which can help improve geomechanical models to be built for the VM.

Basin floor and slope environments were identified for the VM with unique characteristics. Rock-physics modeling is used to explain the log response of the VM in terms of rock properties. Anisotropy analysis is utilized to describe the VM as a VTI (transverse isotropic with a vertical symmetry axis) model. Parasequences were implemented to group and interpolate well log and core data. Linear relationships were observed between the stiffness coefficients measured on cores. Parameters of those relations (per parasequence) were used to compute stiffness coefficients where not enough data were available. The VTI model was fully described and anisotropic Young's modulus and Poisson's ratio were estimated.

I found that acoustic impedance may be used to predict the Total organic content (TOC). TOC influences the hydrocarbon pore volume. A methodology is proposed to calculate the anisotropic elastic moduli. The spatial variations of anisotropic elastic moduli impacts the response of the VM under hydraulic fracturing which should be considered in the design of well-related operations. In summary, this research provides tools for locating sweet spots and optimization of well drilling and stimulations operations, which should help unlock this huge resource.

TABLE OF CONTENTS

ABSTRACT	iii
LIST OF FIGURES	vi
DEDICATION	viii
CHAPTER 1 INTRODUCTION	1
1.1 Research Project and general goals	1
1.2 Geology	3
1.3 Study area and data available	4
CHAPTER 2 INTERPRETATION OF PARASEQUENCES: DEFINITION AND VALUE	8
2.1 The need for a new classification for the VM	8
2.2 Parasequence definition	8
2.3 Insights from parasequence tops correlation with seismic	16
2.3.1 Parasequences & their relation with the depositional environment and TOC distribution of the VM	16
2.3.2 Parasequences & fractures	22
CHAPTER 3 PROPOSED METHODOLOGY TO ESTIMATE ANISOTROPIC ELASTIC MODULI	26
3.1 Governing equations	26
3.2 Velocity anisotropy & correlation with rock properties	27
3.3 Definition & parameter estimation of the anisotropic model	30
CHAPTER 4 INTEGRATED INTERPRETATION	43
CHAPTER 5 CONCLUSIONS	54

5.1 Future work	55
REFERENCES CITED	56

LIST OF FIGURES

Figure 1.1	Comparison of the VM with others shale gas/oil plays	2
Figure 1.2	Location & structural features of the Neuquen Basin	4
Figure 1.3	Stratigraphic column for the Neuquen Basin	5
Figure 1.4	Schematic section of the Neuquen Basin	5
Figure 1.5	Illustrative rock properties for the VM sections	6
Figure 1.6	Data available for the study	6
Figure 1.7	Microseismic surface array, Well G	7
Figure 2.1	Well correlation of the VM mechanical clusters determined by Bishop (2015)	9
Figure 2.2	Schematic explanation for the extra zone found in Well B by Bishop (2015)	9
Figure 2.3	Lithostratigraphy vs. Chronostratigraphy	11
Figure 2.4	Lithostratigraphic VM top well correlation	12
Figure 2.5	Parasequence well correlation in MD	13
Figure 2.6	Parasequence well correlation in MD, zoom for the VM section	14
Figure 2.7	Parasequence correlation in TWT	15
Figure 2.8	Interpreted depositional environments from parasequences	17
Figure 2.9	Comparison of TOC estimations, Well A	19
Figure 2.10	Comparison of TOC from Schmoker and from measurements, Well B	20
Figure 2.11	TOC general distribution for slope facies	21
Figure 2.12	Relation between TOC and AI	21
Figure 2.13	Beef observed in an outcrop of the VM	22

Figure 2.14	Natural fractures interpretation for the VM based on FMI log, Well G	23
Figure 2.15	Structural features correlation between P4b-5 and the Tordillo Formation . . .	25
Figure 3.1	Shear wave anisotropy assessment in well logs	29
Figure 3.2	Comparison of acquired and modeled density and sonic logs for the VM . . .	31
Figure 3.3	VTI Schematic diagram	32
Figure 3.4	VTI Stiffness matrix	32
Figure 3.5	Horizontal vs. vertical Poisson's ratios, Well G	35
Figure 3.6	Estimation per parasequence of k_1 coefficient	36
Figure 3.7	k_1, k_2 and k_3 coefficients calculated per parasequence	36
Figure 3.8	Comparison of anisotropic elastic moduli, Well G	39
Figure 3.9	Velocity comparison of compressional and shear waves, Well G	40
Figure 3.10	Approximation of the P-wave velocity at core frequency	41
Figure 3.11	V_p modeled at core frequency, Well G	42
Figure 4.1	Comparison of isotropic with anisotropic elastic moduli, Well G	44
Figure 4.2	Schematic representation of horizontal Poisson's ratio (ν_{horz}). Modified from .	45
Figure 4.3	Schematic representation of horizontal-vertical Poisson's ratio ($\nu_{horz-vert}$). Modified from	45
Figure 4.4	Completion information for Well G	46
Figure 4.5	Integration of anisotropic elastic moduli, dipole sonic and natural fractures, Well G	47
Figure 4.6	Illustration of induced fracture geometries depending on borehole & stress orientations	48
Figure 4.7	Map display of microseismic events, Well G	49
Figure 4.8	Integration of anisotropic elastic moduli with rock properties, stimulation and production tools, Well G	52

To God who guides my life
to the mountains which protect me
to my family who builds my ground
to my friends who supports me
and to my son,
my Master,
the angel who brings light and fun to my life,
Love you all!

CHAPTER 1

INTRODUCTION

The Vaca Muerta Formation (VM) has produced about 50% of the hydrocarbons in Argentina (Legarreta et al., 2005). It is considered the fourth largest shale oil play in the world with an estimated 27 billion barrels of recoverable oil resources (EIA, 2013). Its unconventional development started in 2010. More than five hundred wells are currently producing from the VM, involving eighteen different operator companies. Most of the wells in the VM have a vertical orientation, unlike the standard horizontal North American unconventional wells. Operating companies decided initially to drill vertical wells due to the rock properties variability of the VM and its large thickness (Figure 1.1). However, in response to a better understanding of the reservoir behavior and identification of sweet spots, companies started drilling horizontally at the end of 2014 (Fernandez Badessich et al., 2016).

1.1 Research Project and general goals

The Reservoir Characterization Project (RCP) at Colorado School of Mines has been conducting research and providing the best practices for hydrocarbon production efficiency for more than 30 years. It has gained world recognition because its multidisciplinary approach, a model that has been widely reproduced within the oil business. A German oil company, Wintershall, brought the VM project to RCP a couple of years ago with the general goals of defining what a sweet spot means for the VM and provide methodologies to optimize well-related operations over their licensed area.

RCP experience and North American unconventional expertise have helped built the technical background for the economic design of the VM shale oil play development. Fernandez-Concheso M. (2015) worked on post and pre-stack seismic inversions to supply a tool to characterize the VM and assess rock properties variability. Bishop (2015) developed a mechanical stratigraphy for the VM based on cluster analysis of well logs, which allowed one to evaluate the variability of

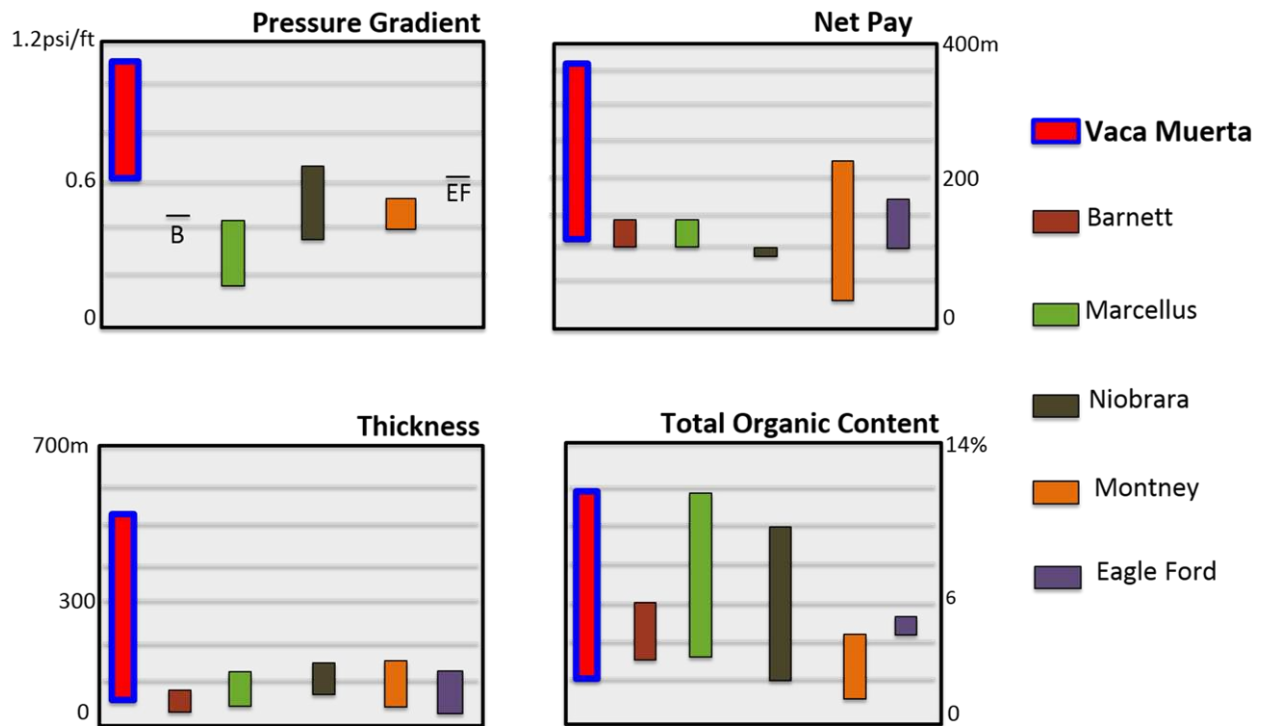


Figure 1.1: Illustrative broad comparison of the VM with others shale gas/oil plays located in the US. Modified from Askenazi et al. (2013).

mechanical properties on the VM and their impact in successful stimulation jobs. Natural fractures were also interpreted and included in the analysis.

The present study has three main objectives: to provide chronostratigraphic tops to properly link well and seismic data, to account for the velocity anisotropy by the estimation of direction-dependent elastic moduli; and to perform an integrated interpretation to show the value of computed moduli to explain stimulation and production of the VM.

Chapter two covers the new classification performed based on sequence stratigraphy to provide chronostratigraphic tops (which were absent) to link well and seismic data. It also shows that the defined time-related strata or parasequences enable one to predict depositional environments for the Quintuco-VM system and their impact on rock properties variability.

Chapter three addresses the velocity behavior of the VM in order to identify rock properties controlling it, and to decide on the anisotropic representation that best describes the VM. It also describes the methodology proposed to estimate anisotropic elastic moduli for the VM.

Chapter four illustrates the information that the estimated anisotropic elastic moduli provide. An integrated interpretation of geology, geophysics and engineering is also presented to characterize and assess the contribution to oil production of different types of fractures and rock properties. Moreover, it reveals the controls on stimulation and production of the VM identified by the computed direction-dependent elastic moduli.

Finally, chapter five concludes highlighting that more accurate calculations of stress state be used in the design of well-related operations for development of the VM.

1.2 Geology

The VM was deposited during the Late Jurassic to the Early Cretaceous in the Neuquen Basin, Argentina. The Neuquen Basin is located in west-central Argentina, east of the Andes Mountain Range, and it is the most prolific basin in Argentina in terms of hydrocarbon production (Legarreta and Villar, 2011). This back arc basin is bounded to the north-east by the Sierra Pintada System and to the south by the North Patagonian Massif (Figure 1.2). The Neuquen Basin has experienced extension during synrift and post-rift phases, and more recently compression, due to a decrease in the subduction angle of the Nazca plate (Kietzmann et al., 2014). The Mendoza group, which includes The VM and its underlying formation for the study area, Tordillo, and overlying formation, Quintuco; was deposited during the post-rift phase.

The Tordillo Formation are continental sandstones deposited over a discordance produced by a major tectonic inversion event. Afterwards, the basin was flooded giving rise to sedimentation of the VM. The VM is a lithostratigraphic unit that corresponds to mid to deep sediments that were deposited in a carbonate low-angle ramp. The VM consists of dark grey, organic rich shales deposited in a low energy and anoxic marine environment (Garcia et al., 2013). Its Total Organic Content (TOC) varies from 2-14%, porosities range from 4-12% and its thickness is about of 250m within the study area. The VM is divided into three sections -Lower, Middle and Upper- according to changes in rock properties. Lower VM has the highest TOC, while Upper VM is considered to be easier to hydraulic fracture. Shale fraction is about 20% and it is rather constant

throughout the formation. The contemporary shallower facies of the depositional system is named the Quintuco Formation. It consists of marls and limestones deposited in the proximal slope/shelf of the carbonate platform (Zeller et al., 2015) (Figure 1.3, Figure 1.4 and Figure 1.5).

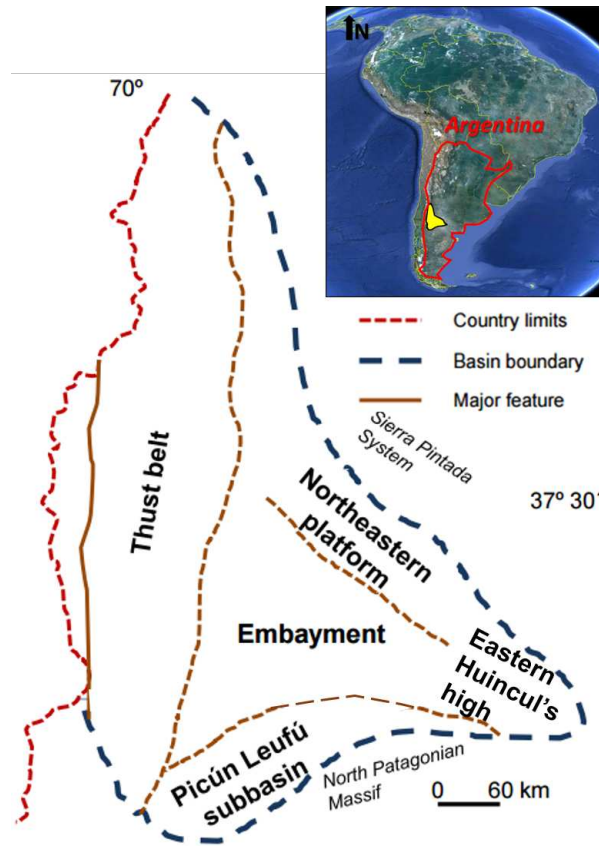


Figure 1.2: Location and structural features of the Neuquen Basin. Modified from (Stinco and Barredo, 2014) and Google Earth.

1.3 Study area and data available

The study area was located in the foreland embayment of the Neuquen Basin, in the black oil window of the VM. A narrow P-wave seismic survey of six hundred squared kilometers, six vertical wells, an entire suite of well logs, core and cuttings measurements were available for this study. Microseismic, completion and production data were also accessible (Figure 1.6).

Available information per well included: standard combo, image logs, spectral Gamma Ray (GR), neutron capture spectroscopy, Nuclear Magnetic Resonance (NMR), dipole sonic and Pro-

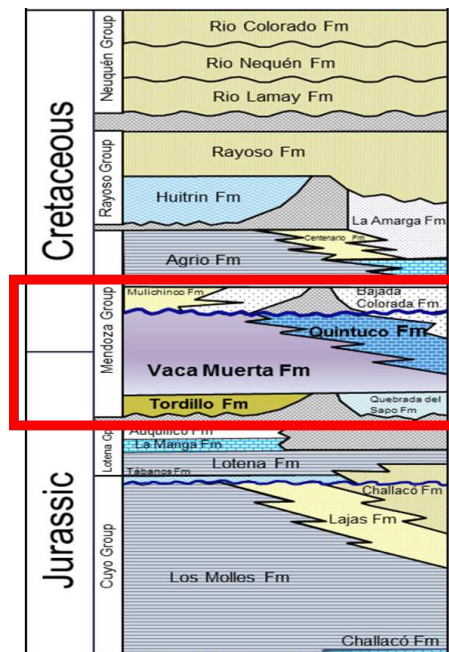


Figure 1.3: Stratigraphic column for the Neuquen Basin. The red box highlights the interval of interest for the present study, which is the Mendoza Group formed by the Quintuco, the VM and the Tordillo Formations. Modified from Howell et al. (2005).

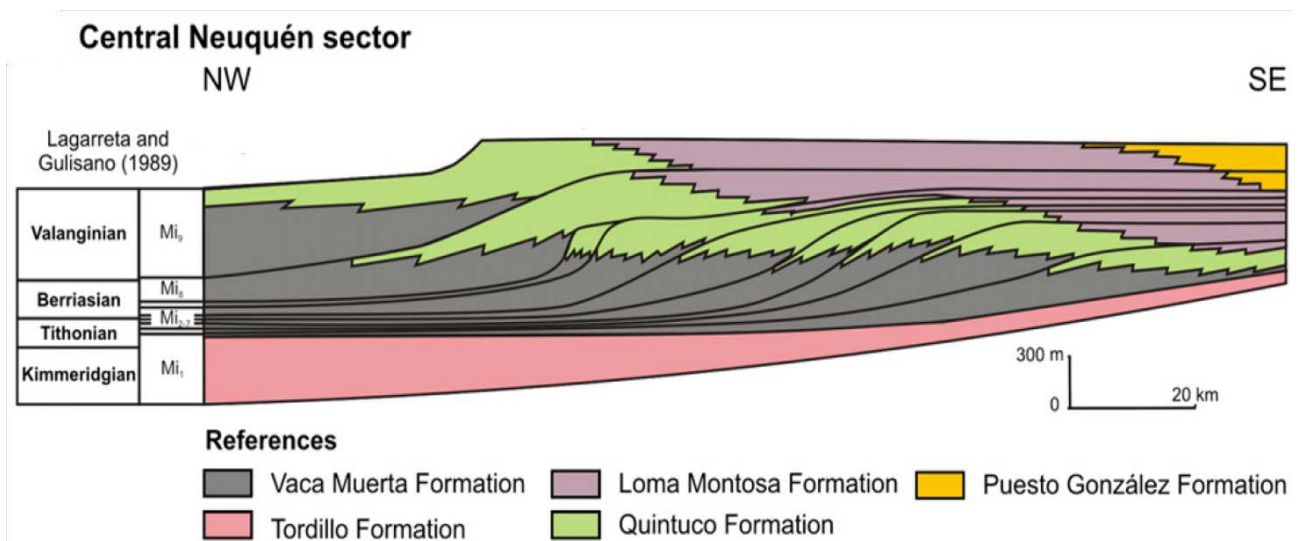


Figure 1.4: Schematic cross-section of Mendoza Mesosequence for the central area of the Neuquen Basin were the study area sits. Modified from Kietzmann et al. (2014).

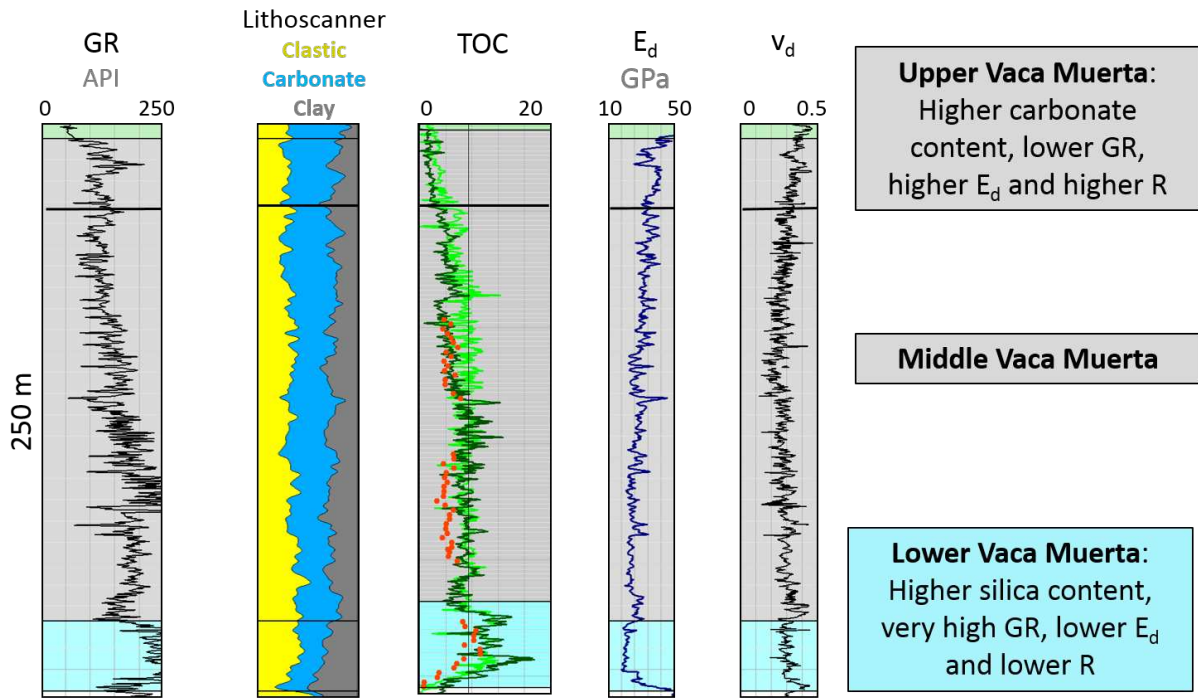


Figure 1.5: Illustrative rock properties and well log behavior for the Upper, Middle and Lower VM sections, within the study area. Modified from Bishop (2015).

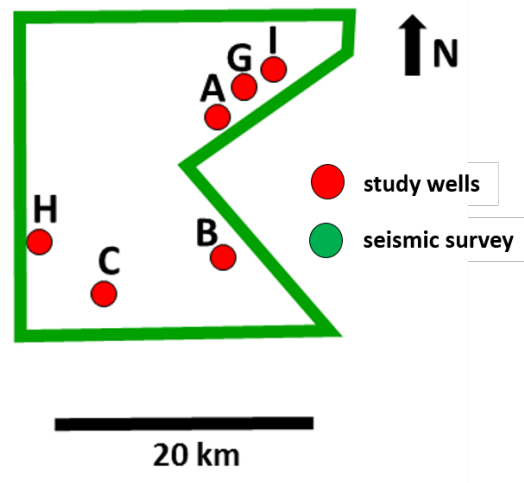


Figure 1.6: Data available for the study.

duction logging tools (PLT). For Wells B, C, and G rock mechanics analysis on core were also accessible.

Surface microseismic was acquired during the hydraulic fracturing of Well G. The FracStarTM array was composed of ten lines of around 3 km length with stations of 12 geophones, placed every 14 m and 2 msec of sample rate (Figure 1.7).

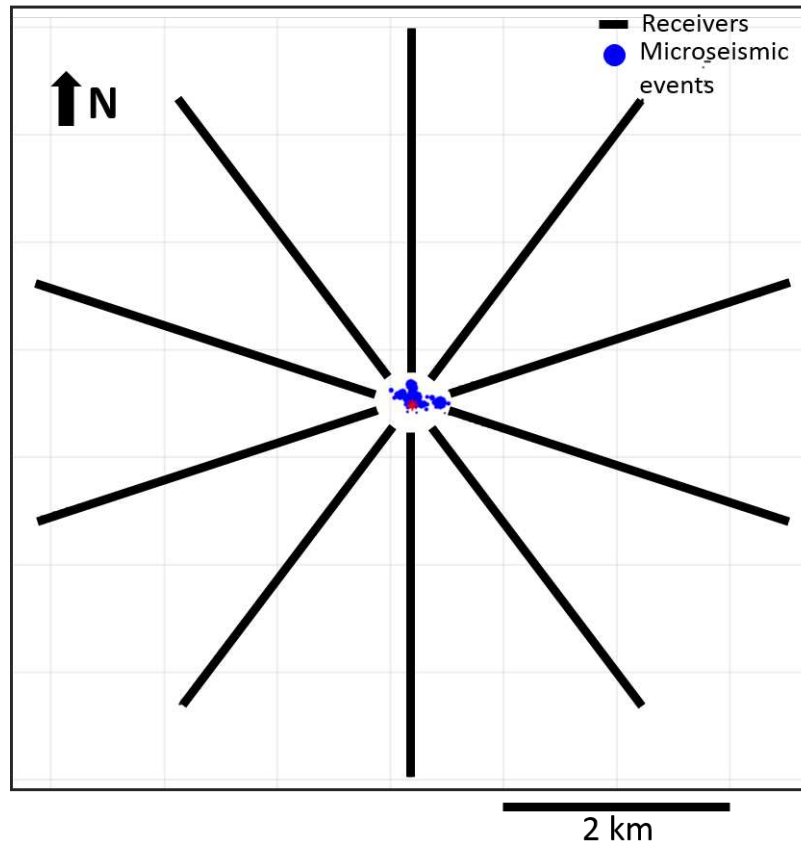


Figure 1.7: Base map showing the surface array deployed for the microseismic acquisition of Well G. From White (2016).

CHAPTER 2

INTERPRETATION OF PARASEQUENCES: DEFINITION AND VALUE

This chapter addresses the new classification developed for the Quintuco-VM system based on depositional environments. The importance of such organization is demonstrated by: accurately connecting well and seismic data through the definition of chronostratigraphic tops; understanding rock properties of the VM by analyzing time-related strata; and, contributing in the development of the anisotropic model of the VM by using the new methodology of facies-based correlation to group and interpolate data.

2.1 The need for a new classification for the VM

Bishop (2015) derived internal markers for the VM based on the behavior of selected well logs to maximize differences between packages while variances within the same interval were minimized. Such an approach is called cluster theory. It was implemented using the Heterogeneous Rock Analysis module from Schlumberger's software, Techlog. Four wells were selected (A, B, C and G) and five well logs were used (deep resistivity, gamma ray, density, Young's modulus and the ratio of compressional to shear wave velocities). Bishop (2015) ended up with six zones within the VM. Three of the four wells showed five zones. The remaining zone was only identified in Well B. Bishop (2015) interpreted that Wells A, C, and G were at the same distance from the former shoreline at the time the VM was deposited; while Well B was in a closer position which explained the prograding clinoforms found in it (Figure 2.1 and Figure 2.2). This fact highlighted the importance of considering depositional characteristics based on chronostratigraphy to understand the rock property variability of the VM.

2.2 Parasequence definition

The dark grey, organic rich marls with an abundant concentration of *Epistomina viviersae* foraminifera deposited in the carbonate ramp developed during the Late Jurassic to the Early Cre-

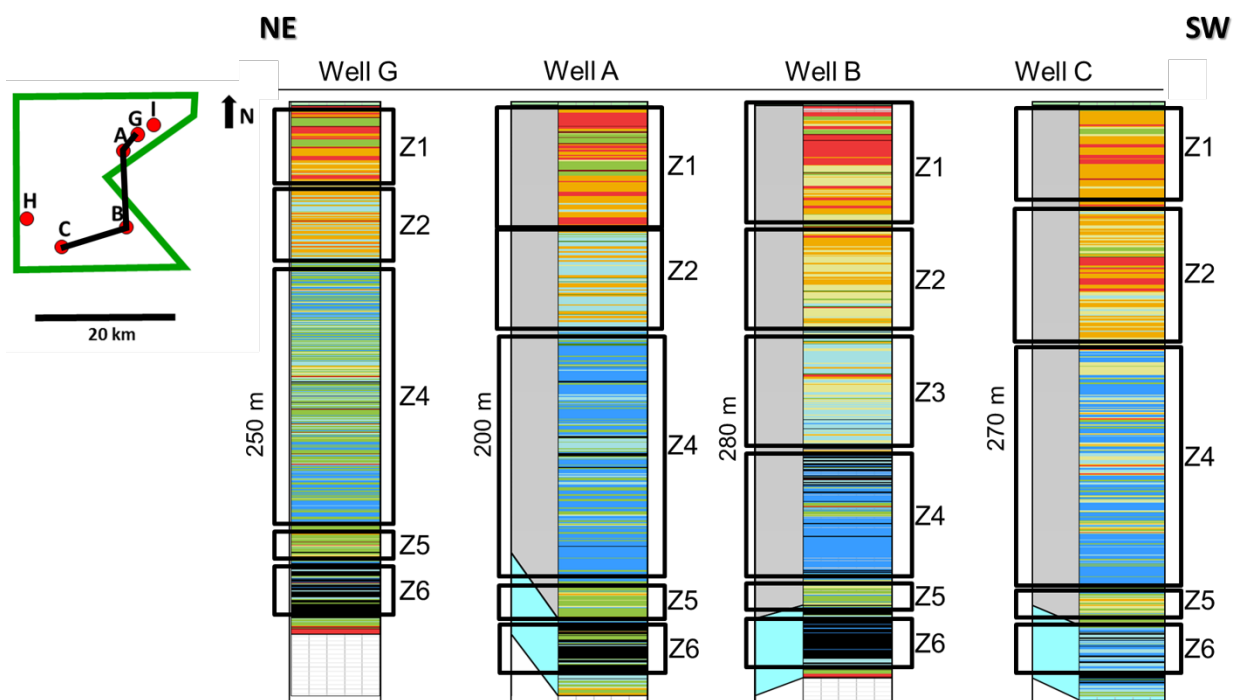


Figure 2.1: Cross-section NE-SW showing the VM mechanical clusters determined by Bishop (2015).

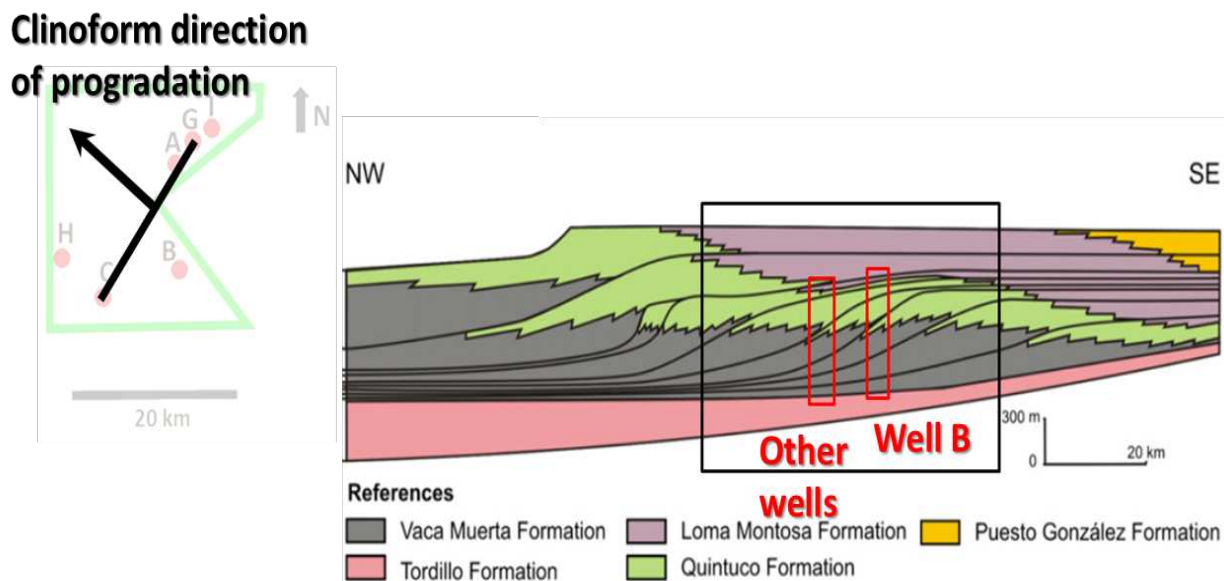


Figure 2.2: Schematic explanation for the extra zone found in Well B. Top left map shows the interpreted progradation direction by Bishop (2015). Cross-section at right, illustrates Well B position in comparison with the other three wells analyzed (Wells A, C and G). Modified from Bishop (2015) and Kietzmann et al. (2014).

taceous in the Neuquen Basin of Argentina are named the Vaca Muerta Formation. This definition is based on type, chemical and fauna characteristics of the VM. Primarily, lithology and geochemistry are used for the interpretation of the top of the VM since they are identified during drilling or logging of this unit, while biostratigraphy requires additional studies. Well correlation based on this approach leads to connect rock packages with similar characteristics deposited at different times. On the other hand, well associations according to rock age -or chronostratigraphy- allows one to investigate rocks that share the same geological history and understand their depositional environments (Figure 2.3). Such methodology could be extended by integrating seismic, provided seismic reflections truly represent time lines which they may or may not do.

As discussed before, chronostratigraphy was not a parameter used for the interpretation of the VM top. The top of VM top did not correspond with a unique seismic reflection that can be mapped and correlated between wells (Figure 2.4). Identification of time-related markers was fundamental to accurately relate well and seismic data. A new classification for the Quintuco-VM system was developed for this purpose using sequence stratigraphy. Sequence stratigraphy uses changes in depositional trends to classify, describe and interpret strata (Embry, 2009). Flooding surfaces are used to correlate units between wells and over the seismic coverage. Marine flooding surfaces limit bedsets genetically related called parasequences (Embry, 2009). Flooding surfaces were defined for the Quintuco-VM system independently for each well based on log character. GR, density and velocity curves were mainly used. Density and velocity logs were specifically implemented because of their direct relation with seismic signature. Synthetics were integrated to build time-depth tables for each well. Well-seismic ties allowed for well-derived flooding surfaces to be displayed over the seismic in two way time (TWT). Flooding surfaces were correlated between wells and ranked to capture rock property variability within the seismic resolution. Finally, eight parasequences were interpreted and named P1 to P8, from the base of the VM -Tordillo Formation- to the top of the Quintuco Formation (Figure 2.5, Figure 2.6 and Figure 2.7).

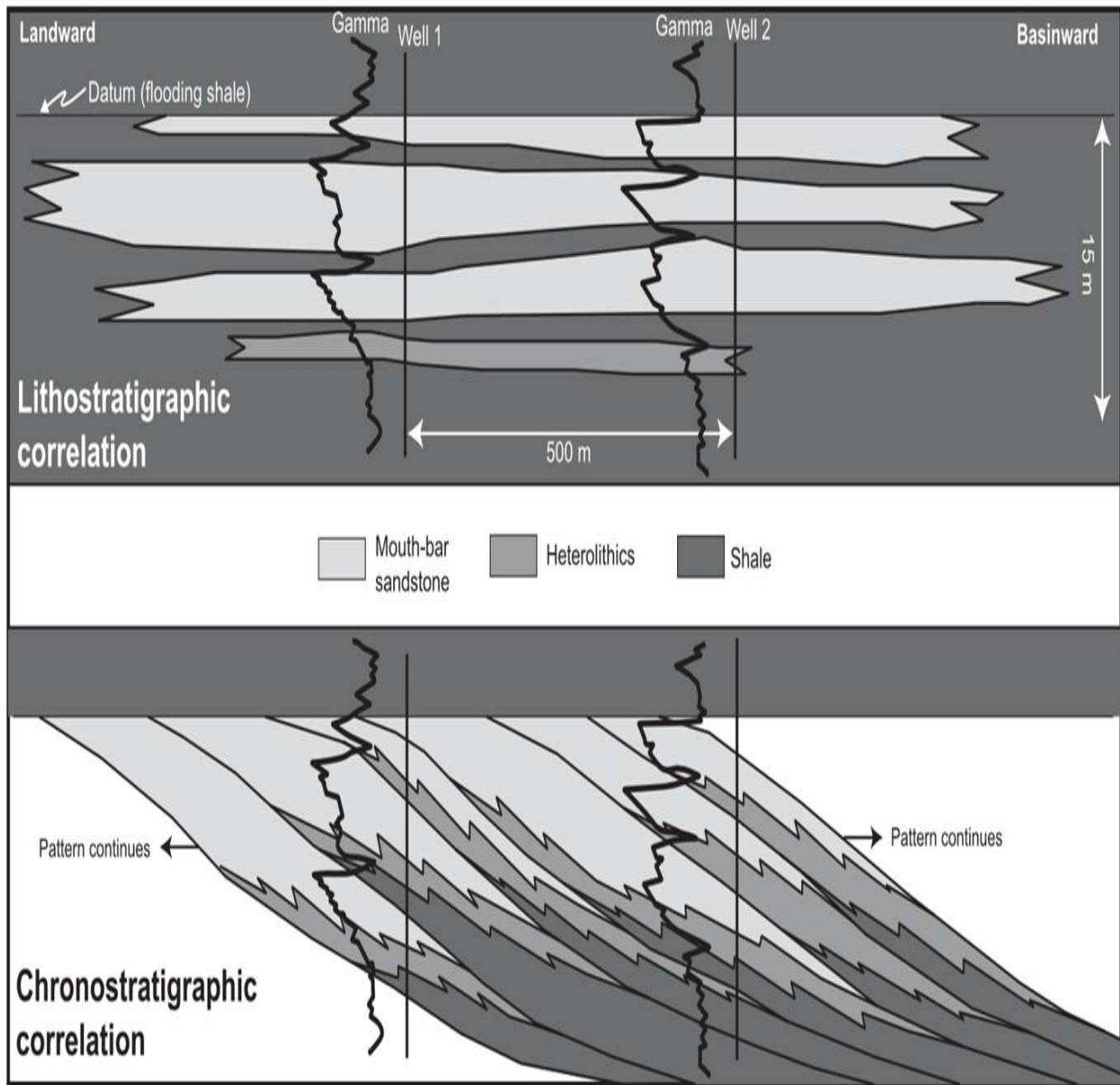


Figure 2.3: Schematic lithostratigraphic versus chronostratigraphic well correlation. Differences can be identified between performing a rock association based on properties or age of the rock, respectively. From Gani and Bhattacharya (2005).

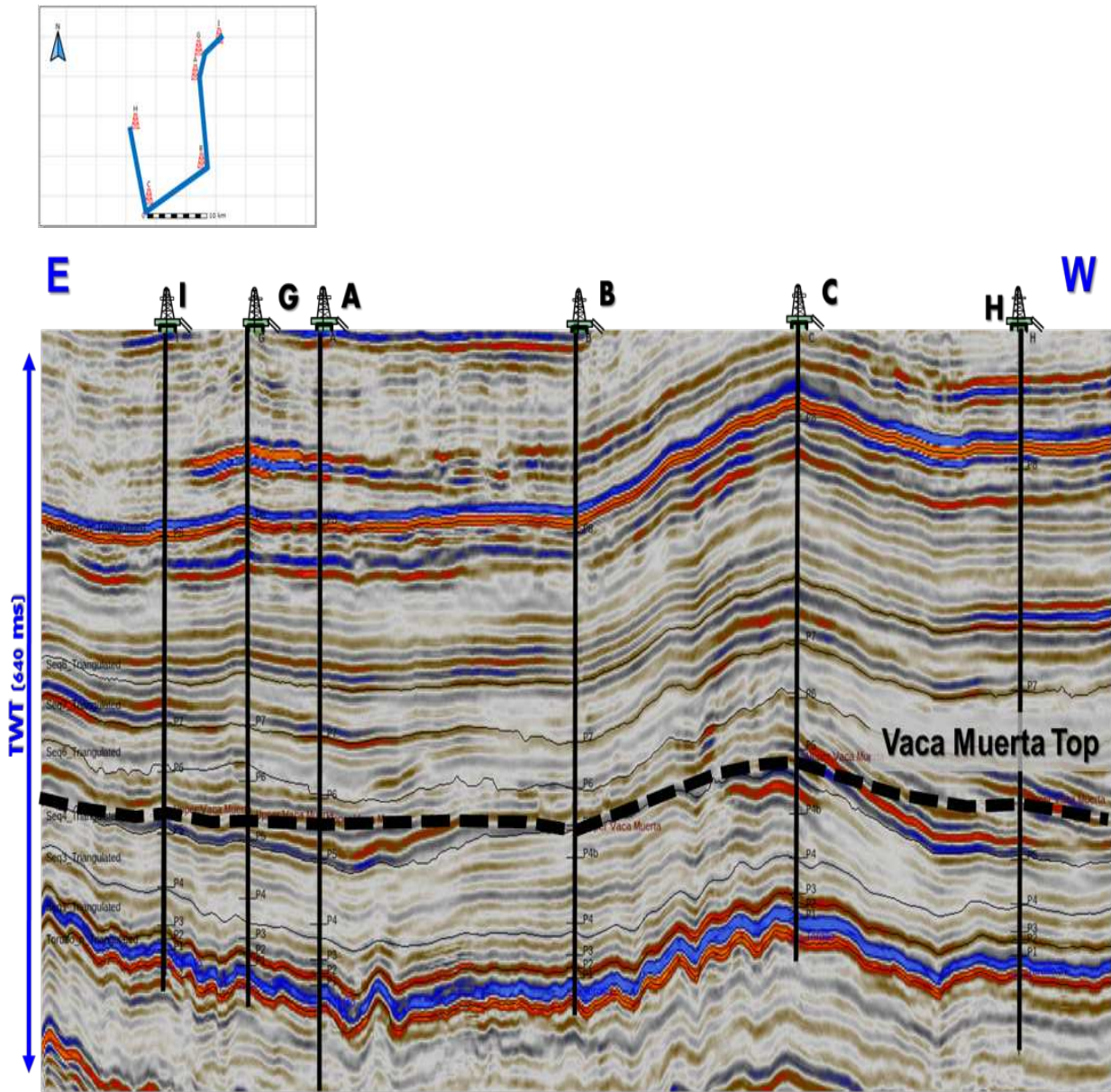


Figure 2.4: VM top well correlation showing that it is not a chronostratigraphic marker. Arbitrary seismic line along study area displaying the wells in black solid lines and the VM top in a black dashed line.

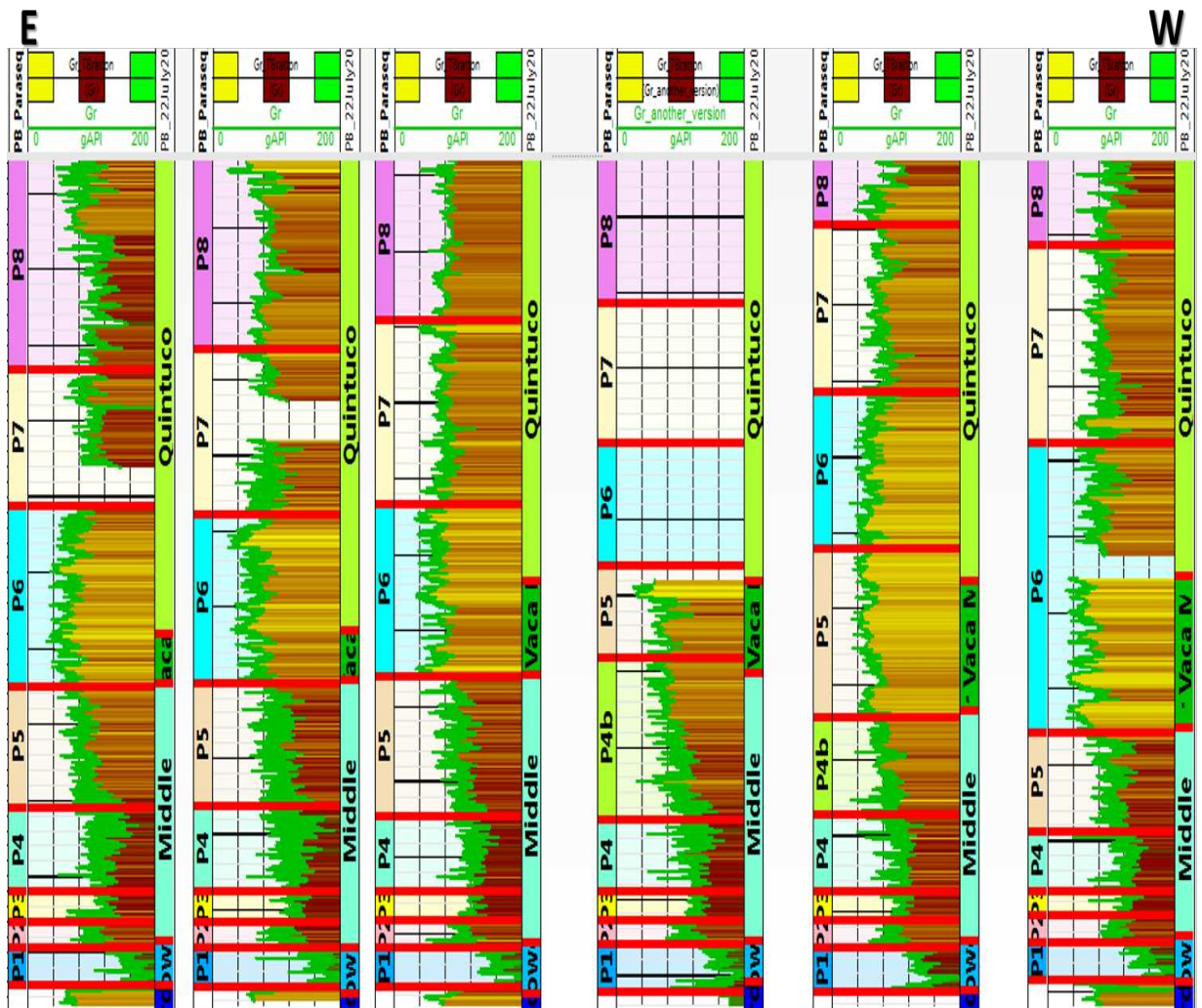
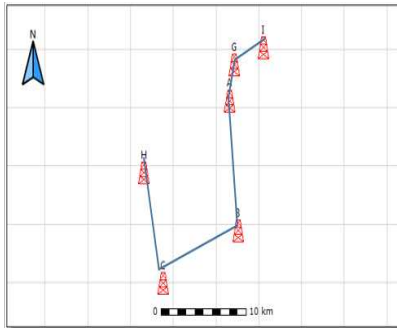


Figure 2.5: Well cross-section from East to West showing the correlation of parasequences for the study area. Marine flooding surfaces are displayed in red-colored lines over GR logs.

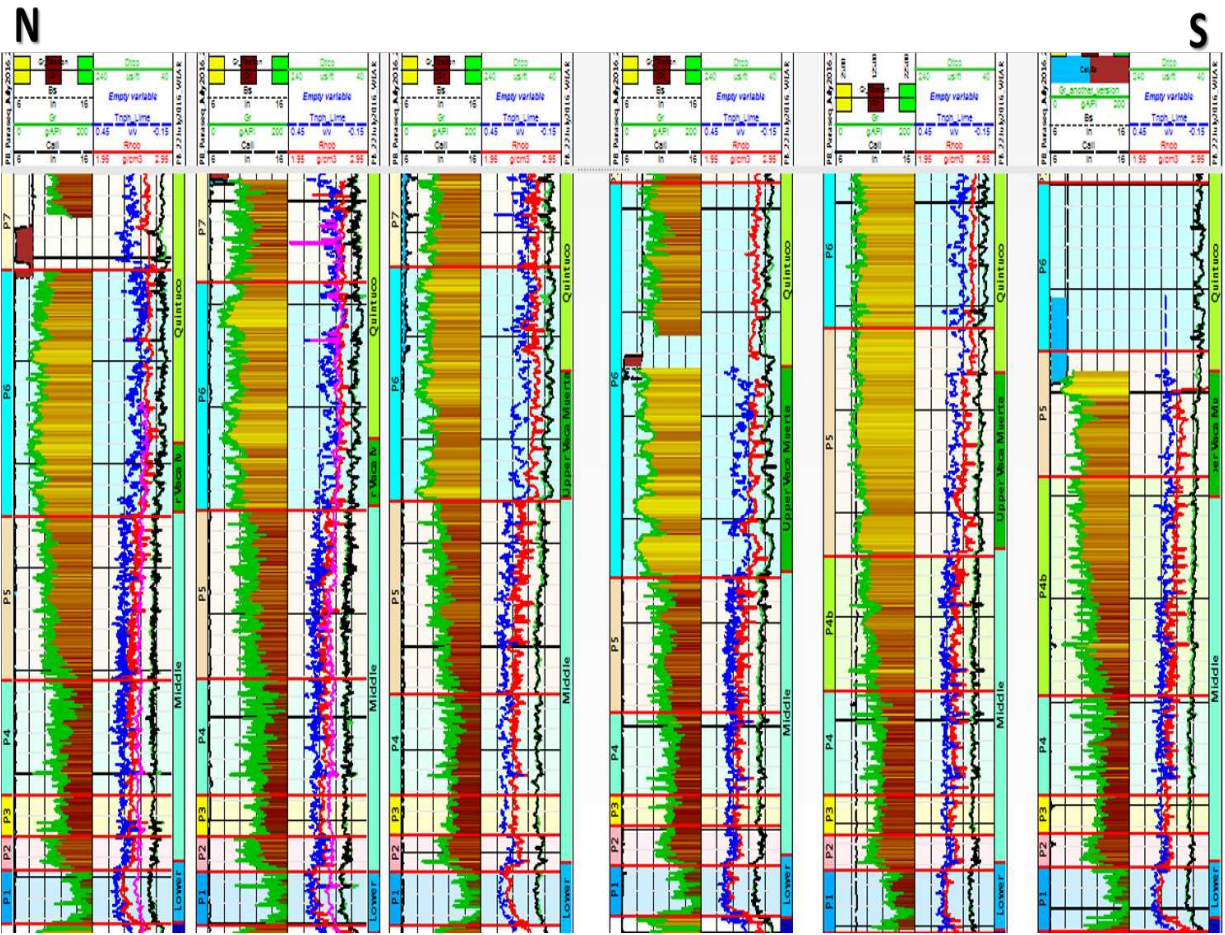
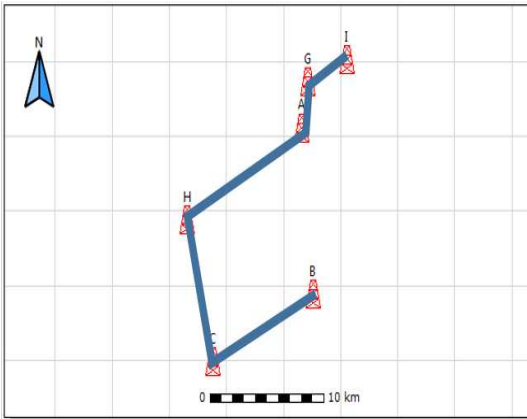


Figure 2.6: Well cross-section from North to South displaying the correlation of parasequence for the study area, focus on the VM section. Marine flooding surfaces are shown in red-colored lines. Right track corresponds to GR log. Left track presents limestone based Neutron Porosity (Tnph.Lime) in blue, density (RhoB) in red, Compressional wave slowness (Dtco) in green, Shear wave slowness (DtSM) in black and Magnetic Resonance Porosity (MRP) in pink

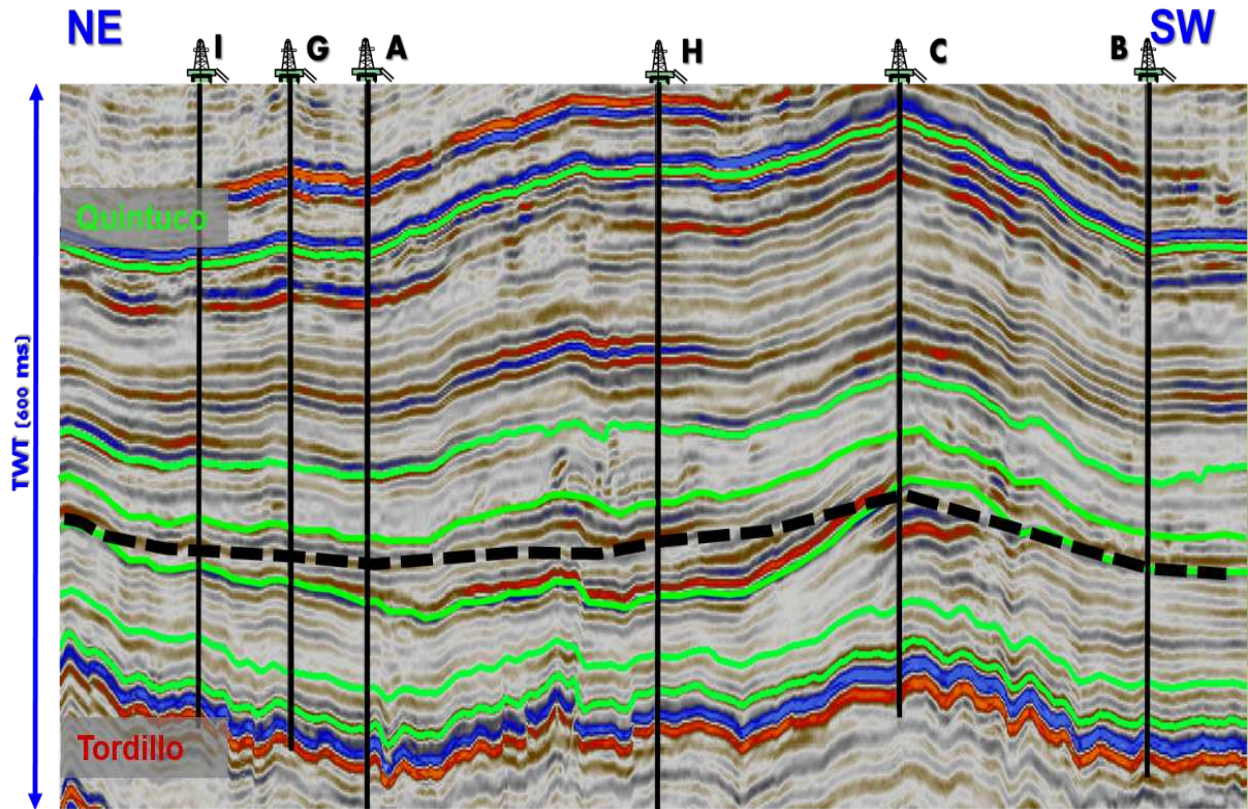
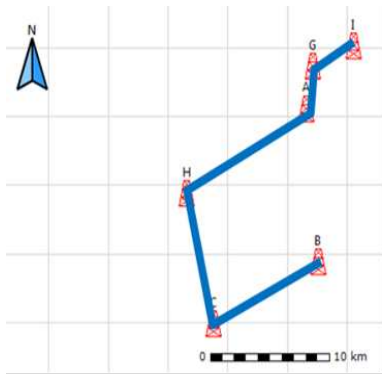


Figure 2.7: Well and seismic parasequence correlation in TWT. An arbitrary seismic line within the study area display the wells in black solid lines and the interpreted parasequences with green solid lines and the VM top with a dash black line. The Quintuco and Tordillo tops are shown at the top and bottom of the figure with the uppermost green line and the deepest red seismic reflection, respectively.

2.3 Insights from parasequence tops correlation with seismic

Parasequence tops were associated with the seismic horizons interpreted by Wintershall to generate isochrons or three-dimensional representations of time-related strata. These 3D parasequences are mapped throughout the study area. The understanding of depositional environment, TOC distribution and structural features gained from their identification is illustrated below.

2.3.1 Parasequences & their relation with the depositional environment and TOC distribution of the VM

Parasequence definition allowed me to depict three main depositional environments within the VM-Quintuco system with unique characteristics. They were basin, slope and shelf settings (Figure 2.8). Parasequences 1 to 4 corresponded to concordant-parallel reflections that could be followed over the study area and found in all wells. They were interpreted as deep water facies deposited on the basin floor. A maximum flooding surface (MFS) was identified at the base of P1 or the base of the VM, top of the Tordillo Formation.

A major change in the internal seismic signature of the interpreted parasequences was identified between parasequences 1-4 (basin floor facies) and parasequences 4b-7. While parasequences 1 to 4 showed concordant-parallel reflections; parasequences 4b to 7 exhibited sigmoidal prograding clinoforms and downlap surfaces. Time lines were equivalent to lithofacies for parasequences 1 to 4, and they were oblique to lithofacies for parasequences 4b to 7. Therefore, parasequences 4b to 7 were interpreted as slope facies and the top of parasequence 4 (which marked the change in the depositional environment) was established as a sequence boundary (SB). The isochron for slope facies (parasequences 4b to 7) demonstrated that the coast line was parallel to the NE-SW direction and it migrated toward the NW. The VM top is located somewhere within P5 and P6, since its definition was based on aspects different from chronostratigraphy, as explained earlier. The top of parasequence 7 corresponded to the base of the Quintuco Formation and it was considered a MFS. It was correlated with the transition between slope and shelf environments. Finally, parasequence 8 encompassed concordant and sub-parallel reflections, in general. Discontinuous and slightly mounded seismic reflections were identified toward the top of the interval, which are related with

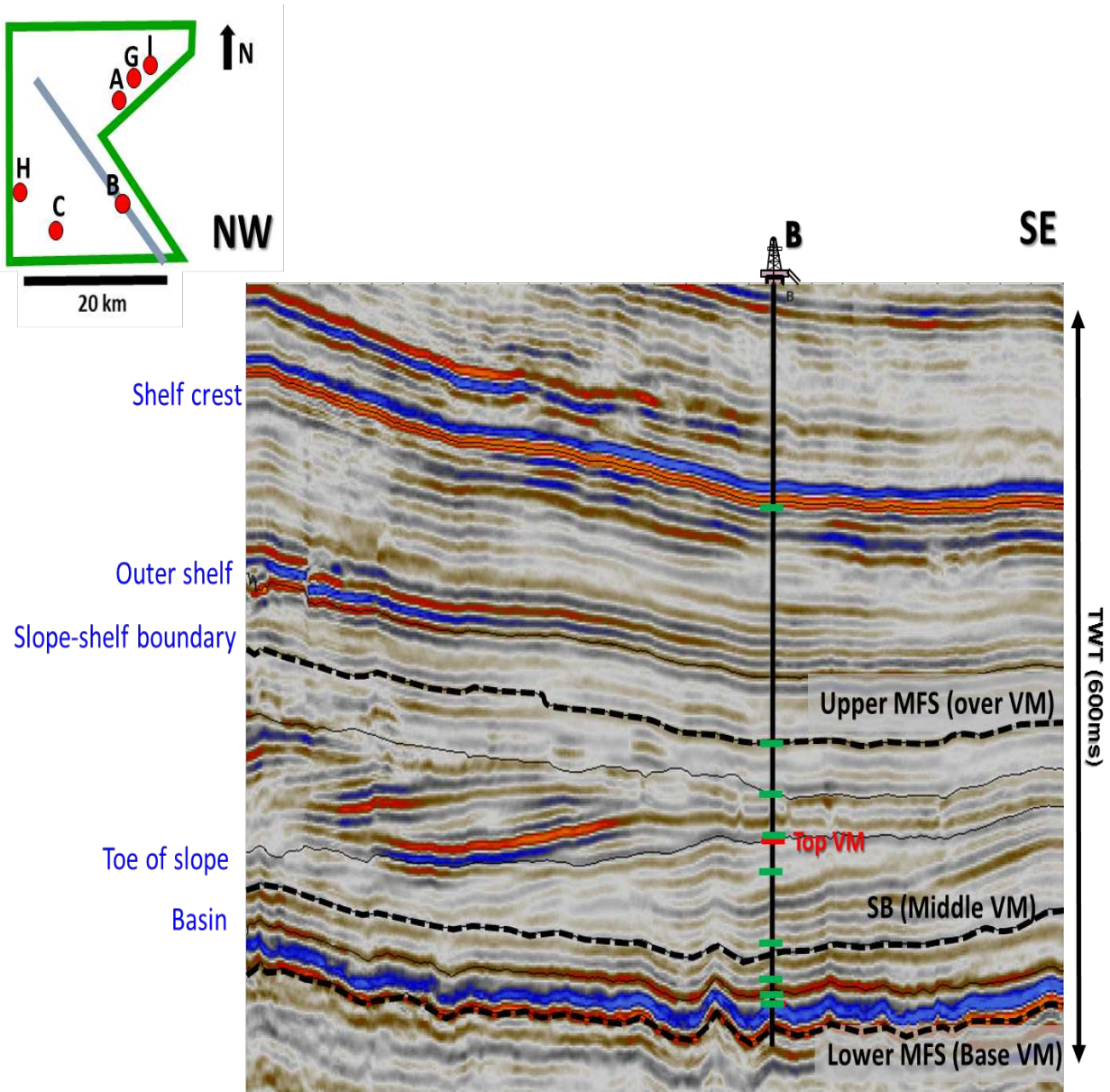


Figure 2.8: Interpreted depositional environments depicted from the described parasequences. Cross-section NW-SE showing the parasequence markers with green ticks and the associated seismic horizons interpreted by Wintershall with solid black lines. The identified MFS's, SB, and depositional environments for the VM-Quintuco system are also displayed with black dashed lines and blue letters, respectively.

shelf deposits.

TOC was evaluated from different well logs. Two methodologies to estimate TOC from well data were assessed, dlogR (Passey et al., 1990) and Schmoker empirical equations (Schmoker, 1979) (Figure 2.9). Measurements of TOC on core, sidewall core and cuttings were available for Wells C and B to validate empirical estimations of TOC. DlogR is shown to be a pessimistic method. A calibrated version of Schmoker was appropriate for the study area. It was used either as an estimation of TOC or to verify TOC evaluated from the litho-scanner tool (Figure 2.10).

Analysis of the TOC response depending on the depositional environment of the Quintuco-VM system demonstrated a high TOC variability within the slope facies, parasequences 4b to 7. Figure 2.11 showed that rocks drilled in Well G were richer in organic matter content than intervals logged in Well B. The calculated isochron of parasequences 4b to 5 revealed that Wells A, G and H encountered the slope toe areas of the basin, while Wells B and C were located in more shelf proximal environments. TOC behavior was explained in terms of the depositional environment. Deeper areas of the basin had less oxygen and allowed for high concentrations of TOC, as demonstrated in Wells A, G and H. Contrarily, more oxygen was available in locations closer to the shelf observed from TOC values of Wells B and C (Figure 2.11).

Acoustic impedance (AI) was investigated for a possible relation with TOC. AI was estimated using velocity and density logs for the study area wells. AI curve represented a mirror version of the TOC logs. An inverse linear relationship was observed between AI and TOC. As AI decreases, TOC increases. AI and TOC values were colored according to the interpreted depositional environments of the VM. Slope facies exhibited large values of AI and low of TOC while the opposite was true for the basin facies of the VM (Figure 2.12). Therefore, acoustic impedance may be used to predict TOC. Inverted seismic volumes of AI could be utilized to generate cubes of TOC. TOC volumes are important for unconventional sweet spot definition since TOC correlates with porosity and hydrocarbon saturation. Then TOC cubes may contribute to identify zones with large hydrocarbon pore volume.

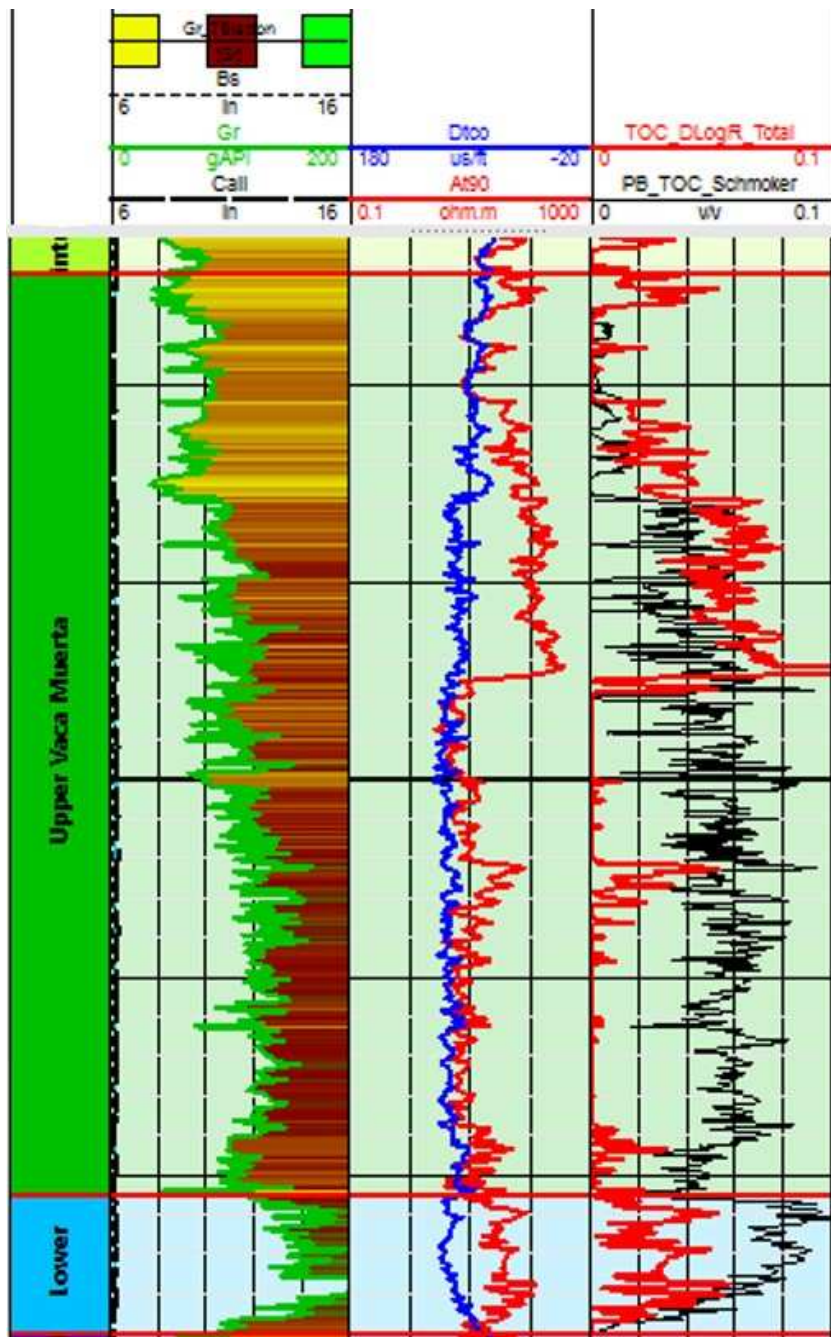


Figure 2.9: Comparison of dlogR and Schmoker TOC estimations for Well A. From left to right are displayed: GR with a green line and a filled pattern in the first track; compressional slowness (D100) and deep resistivity (At90) with blue and red lines, respectively in the second track; and TOC logs derived from dlogR (red line) and Schmoker (black curve) in the third track.

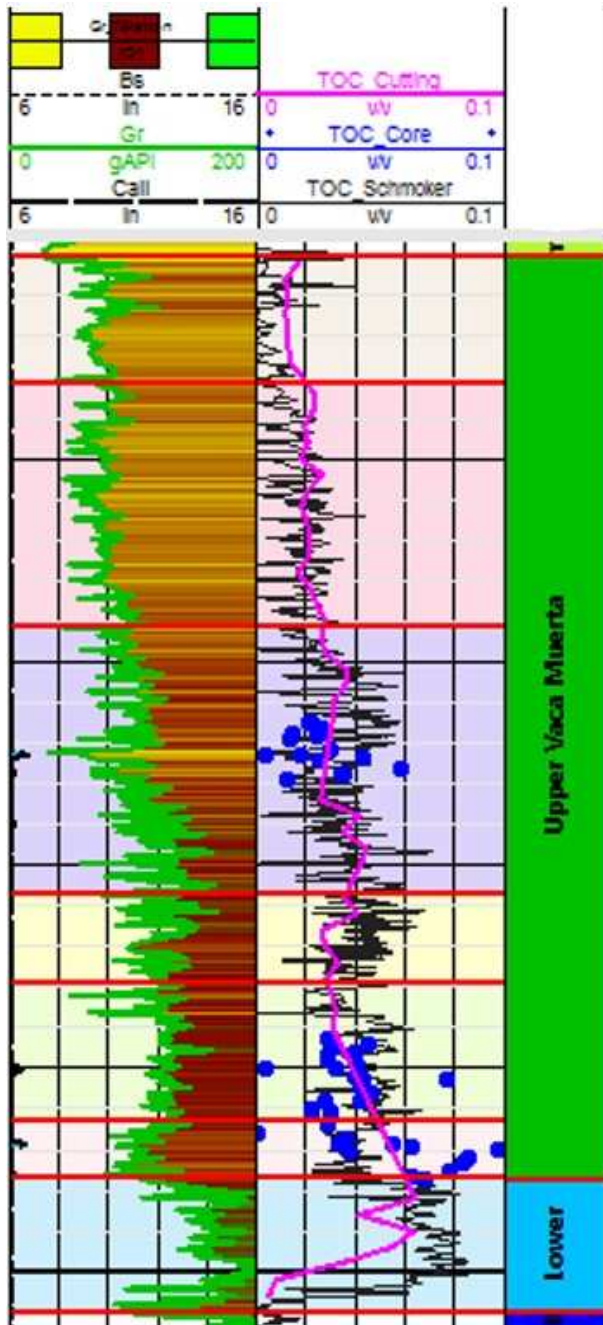


Figure 2.10: Comparison of calibrated Schmoker curve with TOC measurements for Well B. GR is displayed with a green line and a filled pattern in the left track. TOC derived from Schmoker empirical relation (black curve) and measurements of TOC on cuttings (pink line) and on cores (blue circles) are shown in the right track.

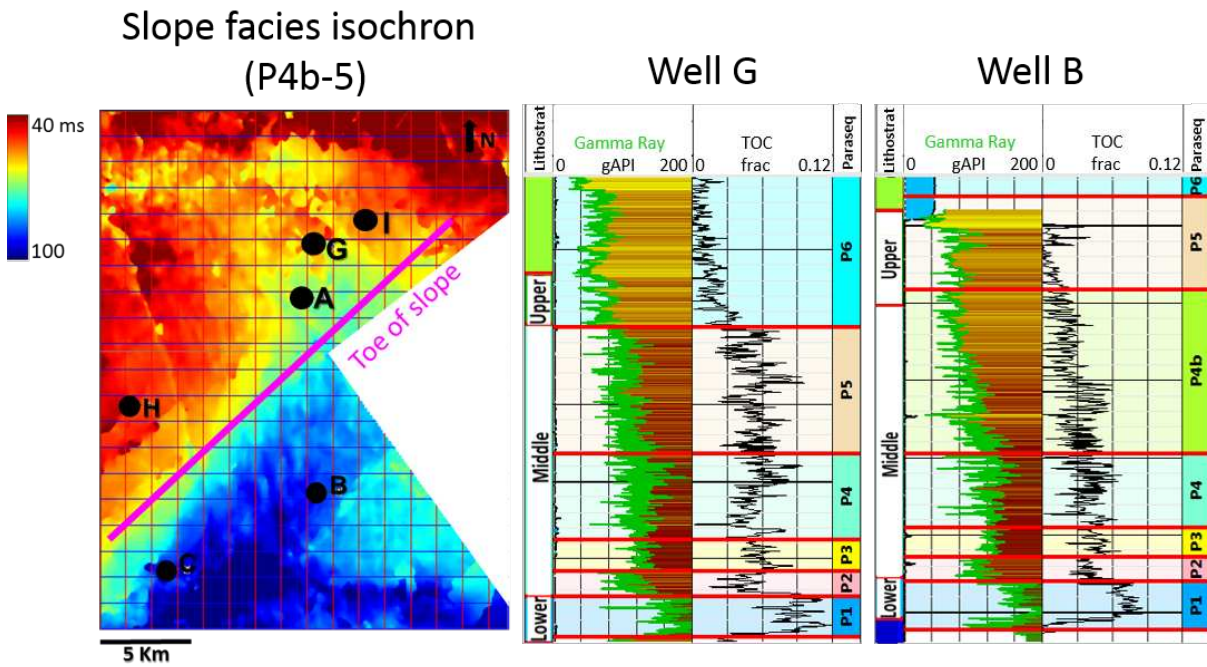


Figure 2.11: TOC general distribution for slope facies. P4b-5 isochron is shown at left. GR (green curve) and TOC (black log) are displayed for Wells G and B.

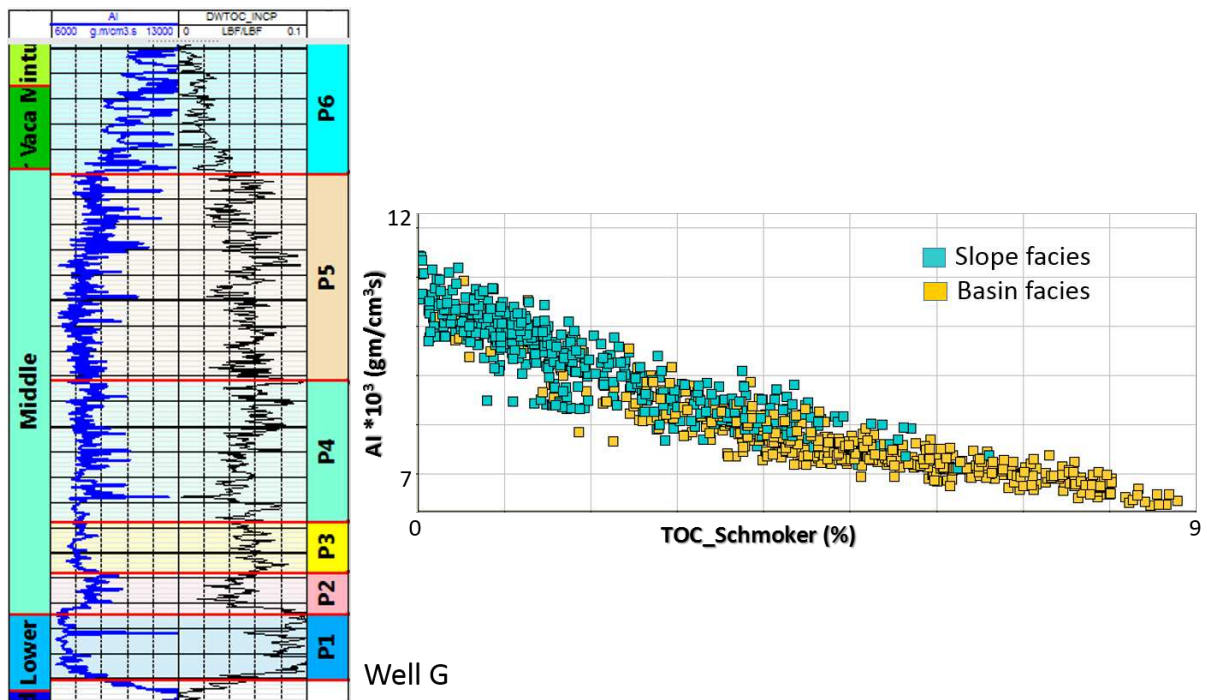


Figure 2.12: Relation between TOC and AI. It can be observed that AI constitutes a mirror image of TOC, left. Crossplot of AI versus TOC evidencing their linear regression, right.

2.3.2 Parasequences & fractures

The VM exhibits high content of organic matter and carbonate. "Beefs" features or bedding parallel veins of fibrous material have been widely described in sedimentary basins rich in organic and carbonate content as the VM (Figure 2.13). The development of horizontal fractures indicates that the vertical stress had to be the lowest, like in trust faulting regimes or in overpressure reservoirs (Bishop, 2015). Besides, fluid hydrocarbon inclusions in beefs has been documented for the VM. It may indicate that the hydrocarbon generation was produced at the same time beefs were created, which can be understood by the high fluid pressures originated by the maturation of kero-gen (Rodrigues et al., 2009a). Study and identification of beefs are fundamental for completion operations, given that beefs can limit the hydraulic fracture area of a stimulated well. Beefs are a hot-topic research in the VM.



Figure 2.13: Beef observed in an outcrop of the VM, Neuquen basin. From Rodrigues et al. (2009a).

Additionally, Bishop (2015) evaluated the formation micro-imager log (FMI) run for Well G to assess the presence of natural fractures. Two main natural fracture sets were identified for the middle section of the VM. One set of highly dipping fractures with orientation N50-230°, and a second set of more gently dipping fractures with orientation N145-325°. Also, a natural fracture

intensity log was created (Figure 2.14). Data from Wells A, B, and C were also analyzed, but they were not conclusive. Wells A, B, and C were drilled with oil based muds and therefore the image logs were of poor quality.

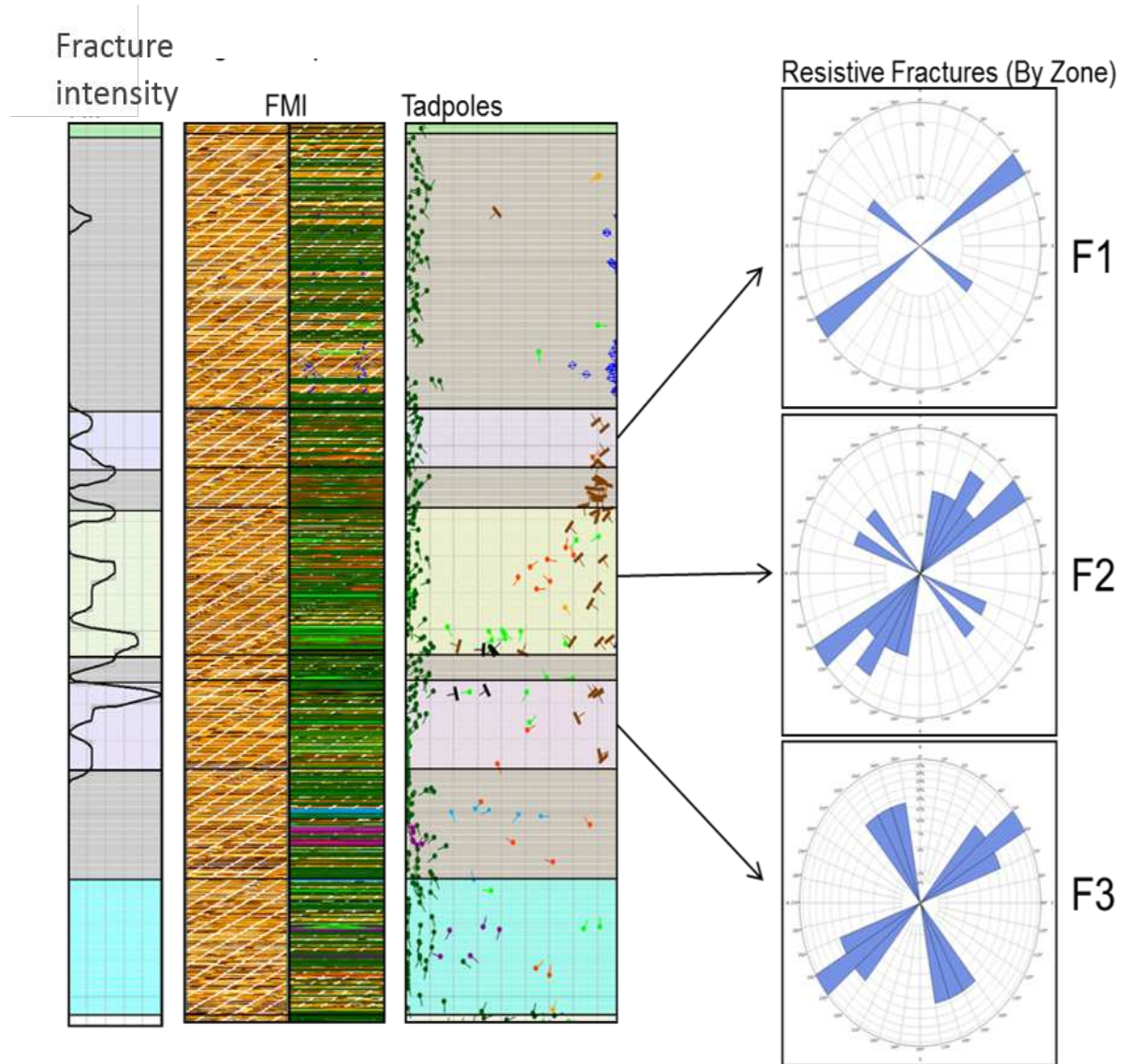


Figure 2.14: Natural fractures interpretation for the VM based on FMI log for Well G. Modified from Bishop (2015).

Garcia et al. (2013) and Sagasti et al. (2014) found that thermal subsidence and sediment influx were almost constant during the deposition of the VM. As a result, changes in depth could be either attributed to tectonics or eustatic level changes. Structural features interpreted on the isochron for

parasequences 4b to 5 suggested that tectonism increased during this period (Figure 2.15). A high correlation was observed between identified structural features on the isochron of parasequences 4b to 5 and the one for the Tordillo Formation, indicating that faulting was active during the deposition of the VM. Furthermore, the orientation of structural features present in the isochron for parasequences 4b to 5 was very similar to the strike of interpreted natural fractures by Bishop (2015) (Figure 2.14). The direction of these two main sets of natural fractures was N50° and N145°. The orientation interpreted for the present maximum horizontal stress was E-W (N90°). Therefore, neither faulting nor natural fractures are aligned with the current maximum horizontal stress. Mosquera and Ramos (2006), among others, documented a maximum horizontal stress of NW-SE during the Mesozoic, and a later rotation during the Cenozoic to the present direction, which is E-W. The former orientation of the maximum horizontal stress explained the structural features described for the VM and the Tordillo Formations. Consequently, natural fractures identified for the middle section of the VM were related with a former stress regime. Moreover, Bishop (2015), Rodrigues et al. (2009b) and others, have suggested that the process of hydrocarbon generation could be playing a role in the occurrence of natural fractures.

Parasequences described the horizontal relation between genetically related bedsets according to their depositional environment. They provided chronostratigraphic tops for the VM that allowed me to accurately link well and seismic data. They also contributed to explain the TOC variability and structural features present in the VM. Additionally, parasequences were used to group and interpolate core data to build the anisotropic model for the VM -as it will be described in the next chapter. Moreover, they were implemented to create low-frequency models for seismic inversions. In summary, a parasequence interpretation was the basis for my study.

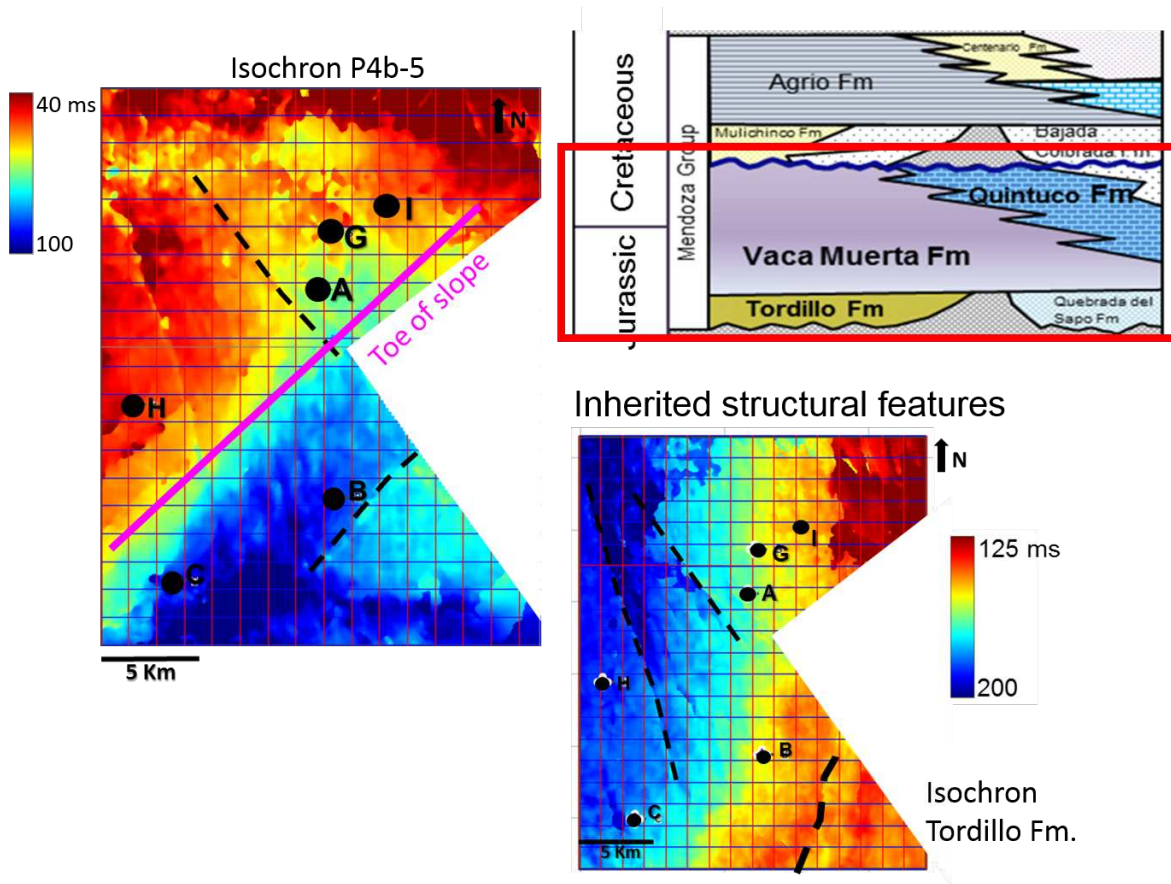


Figure 2.15: Correlation between structural features identified for P4b-5 isochron and faults seen in the Tordillo isochron. Left map shows the isochron of P4b-5 with some structural features interpreted (black dashed lines). Right bottom map displays the Tordillo isochron in which faults with directions very similar to the ones in the VM are observed. An extract of the stratigraphic column (Howell et al., 2005) is exhibited at the top right corner to illustrate the stratigraphic relation between the VM and the underlying Tordillo Formation.

CHAPTER 3

PROPOSED METHODOLOGY TO ESTIMATE ANISOTROPIC ELASTIC MODULI

This chapter presents a methodology to estimate anisotropic elastic moduli to more accurately compute stress state and guide definition of preferable zones to stimulate according to the heterogeneity of the calculated moduli. First, general laws are analyzed to explain the role of the stiffness matrix in the definition of the stress state of a reservoir. Second, the velocity anisotropy assessment of the VM guides the anisotropic modeling. Third, the methodology proposed to compute anisotropic elastic moduli is explained. Finally, rock-physics model describe velocities and density log behavior of the VM in terms of lithology, TOC and overpressure.

3.1 Governing equations

Hooke's law states that the force needed to extend or compress a spring by some distance depends on that distance. The generalized form of Hooke's law relates the strain of a material with the stress applied to it. Strain could be expressed in terms of displacement vector. Then the generalized form of Hooke's law could be written as below:

$$\tau_{ij} = c_{ijkl} \frac{\partial u_k}{\partial x_l} \quad (3.1)$$

A critical component of the generalized form of Hooke's law is the stiffness tensor (c_{ijkl}), which relates stress and strain. The form of the stiffness tensor depends on the material properties. It can be represented as a 6x6 matrix by implementing the well-known *Voigt notation*. The number of independent parameters of this matrix is governed by the symmetry of the system. 21 parameters are needed to describe a model with the lowest possible symmetry. This representation is known as triclinic and it is difficult to implement due to the large number of parameters. Subsequently, monoclinic models have a plane of mirror symmetry by which the amount of independent variables are reduced to 13. Orthorhombic representations have two more mirror planes of symmetry than the monoclinic's. As a result, nine independent parameters should be found to describe them.

Transversely isotropic media (TI) have been widely studied and implemented because just five independent parameters have to be defined with a known axis direction. They have an axis of rotational symmetry. According to the orientation of this rotational symmetry axis, TI models are called VTI for vertical axis direction and HTI for transverse isotropy models with a horizontal axis. Lastly, the stiffness matrix of an isotropic medium has just two independent parameters (Tsvankin, 2012).

3.2 Velocity anisotropy & correlation with rock properties

The behavior of the velocity with direction of the VM for P and S-waves was analyzed. It allowed to decide the anisotropic representation for the VM. It also enabled the identification of rock properties controlling the velocity response of the VM.

Dipole sonic and Stoneley data were used for the velocity assessment. In terms of rock properties, TOC was evaluated from a litho-scanner tool response and clay content was calculated from the petrophysical evaluation performed by Wintershall's petrophysicist, Pablo Pateti, in August 2016. Correlation of the velocity behavior with natural fractures present in the VM was also investigated. The interpretation carried out by Bishop (2015) was used (See Chapter two, section 2.3.2).

The dipole sonic run on Well G provided information about the slow and fast S_V -wave velocities. Fast to slow S_V -wave velocity ratio was computed (Figure 3.1 left track, V_{sFast}/V_{sSlow}). Values were close to unity, indicating that fast and slow S_V -wave velocities were very similar. Such minimum S_V -wave splitting phenomena observed in spite of the presence of natural fractures may be explained by the fact that the vast majority of the identified dipping fractures were interpreted as closed fractures. Bishop (2015) recognized 28 fractures within the 240m thick of the VM, in Well G. 24 of those fractures were classified as healed or closed. In agreement to this, core photos and thin sections showed that most of the fractures present in the VM are healed with calcite cement. These facts explain the similarity between fast and slow values of S_V -wave velocities for the VM.

Stoneley data were used to compute the horizontal S_H -wave velocity. Wintershall implemented the (White, 1983) equation to achieve that goal. V_{ST} is the velocity of the Stoneley wave, V_{S_H} is the velocity of the horizontal S_H -wave, ρ is the density of the formation, and V_f and ρ_f are the velocity and density of the fluid in the borehole, respectively.

$$V_{ST} = \frac{V_f}{\sqrt{1 + \frac{V_f^2 \rho_f}{V_{S_H}^2 \rho}}} \quad (3.2)$$

The ratio between the vertical and horizontal S-wave velocities was calculated (Figure 3.1 pink curve middle track, V_{s_vert}/V_{s_horiz}). Vertical and horizontal S-wave velocities had similar values for lithostratigraphic units underlying and overlying the VM, the Tordillo and the Quintuco Formations, respectively. Thus, the vertical to horizontal S-wave velocity ratio was close to unity for the Tordillo and the Quintuco Formations. The horizontal S-wave velocity generally increased with depth at a higher rate than the vertical S-wave velocity within the VM. Consequently, the vertical to horizontal S-wave velocity ratio slightly decreased with depth for most of the VM. The horizontal S-wave velocity was up to 25% larger than the vertical shear counterpart for the lower VM, parasequence 1, located in the basin facies.

An inverse correlation was observed between the vertical to horizontal S-wave velocity ratio and the TOC of the VM. The vertical to horizontal S-wave velocity ratio decreases as TOC increases. On the other hand, clay content by itself cannot explain observed differences between vertical and horizontal S-wave velocities. Because clay content is consistent throughout the VM, increasing slightly for the upper half of the VM (Figure 3.1).

Relationships were identified between the velocity response of P and S-waves and TOC, in well logs. Therefore, a rock-physics model was built to obtain more information about the effects of TOC and lithology in the velocity and density behaviors of the VM. Mineral fractions of quartz, calcite, kerogen and pyrite were mixed using Reuss law to create the matrix. Clay parameters were based on Tosaya (1982), Han (1987) and illite values since it was the main clay type in the VM. Pressure Versus Temperature (PVT) fluid analysis and Batzle and Wang (1992) simplified equations were employed to determine the acoustic properties of the fluids, in this case oil and wa-

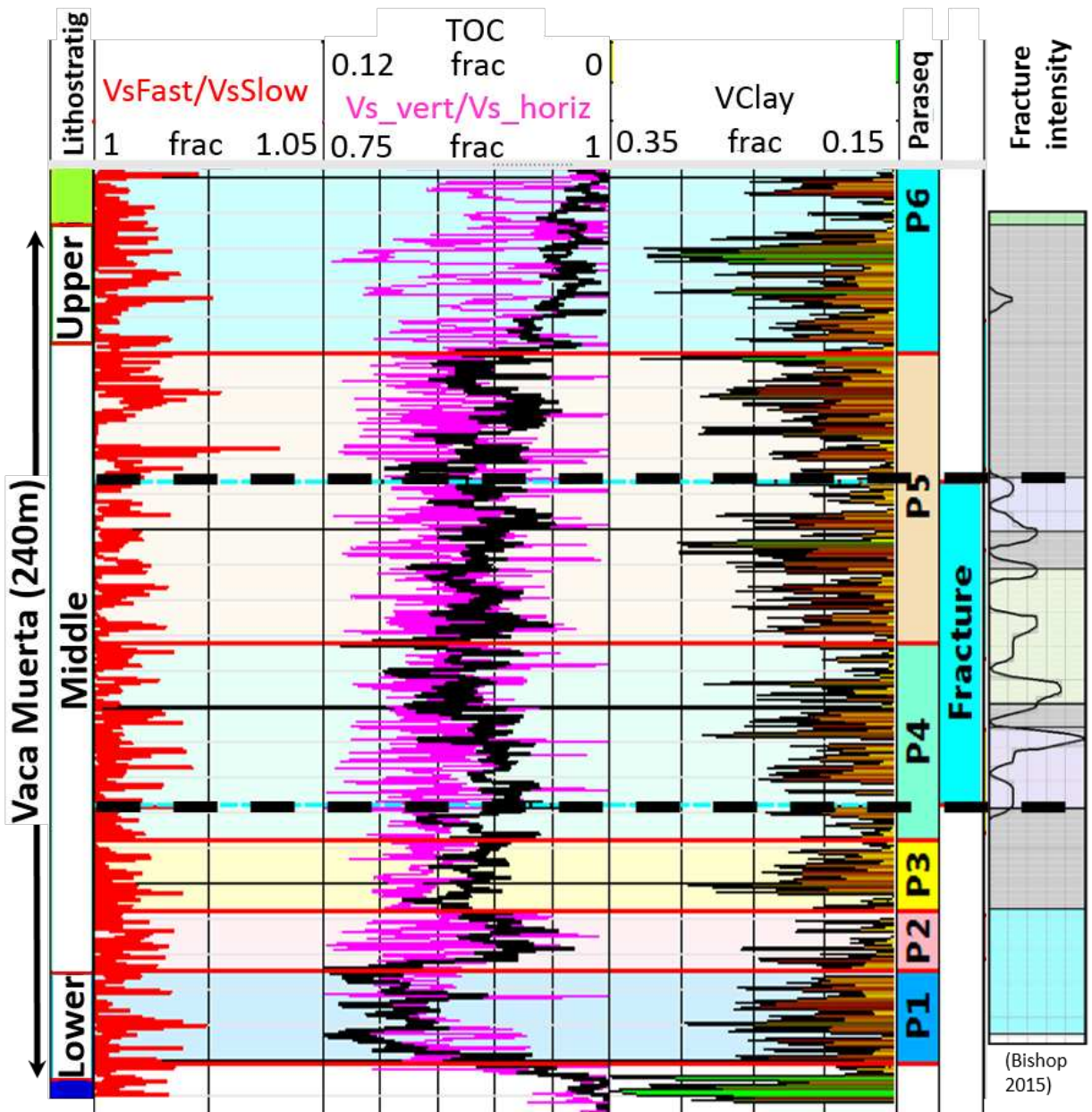


Figure 3.1: Assessment of S-wave velocity anisotropy at log scale for Well G. From left to right, the first track shows in red color the fast to slow S-wave velocity ratio (V_{sFast}/V_{sSlow}). Vertical to horizontal S-wave velocity ratio (V_{s_vert}/V_{s_horiz}) is displayed in pink color, on the second track. TOC derived from litho-scanner tool is over V_{s_vert}/V_{s_horiz} in black color; clay content is on the third track and natural fracture intensity from Bishop (2015) is on the rightmost track. Lithostratigraphic and Parasequence tops are also presented.

ter. These properties were combined using saturation values from the petrophysical interpretation performed by Wintershall's petrophysicist, Pablo Pateti, in August 2016. The mixed matrix was unified with clay using Upper Hashin-Shtrikman law. Fluids were combined by applying Woods law with an exponent of one. Five percent of calcite cement was assumed to build a contact cemented model. And, a linear pore pressure gradient was used since it agreed with pressure tests performed in Well G.

Figure 3.2 shows that density and sonic responses are replicated with the rock-physics model described. A minor mismatch can be observed for parasequence 1, Lower VM, where the modeled data exhibits larger values than the acquired values. The percentage of calcite cement was reduced from five to three percent for this parasequence and a good tie was achieved. Such reduction in the amount of calcite cement was explained by the increase in kerogen given that parasequence 1 was the interval with the highest TOC within the VM. TOC effect on density and P and S-wave velocities was confirmed. Rock-physics modeling explained why TOC could be predicted from acoustic impedance, as it was shown in Chapter two, section 2.3.1. This finding is very important since TOC influences hydrocarbon pore volume. Then, inverted seismic cubes may be used to generate TOC volumes to contribute in the sweet spot definition of the VM.

3.3 Definition & parameter estimation of the anisotropic model

Previous section demonstrated similar values for the slow and fast S_V -wave velocities of the VM. Differences between the vertical and horizontal S-wave velocities were also documented. Therefore, the velocity response of the VM may be described by the implementation of a vertical transverse isotropic or VTI model, according to the information available (Figure 3.3).

VTI representations require five independent parameters to fully describe P and S-wave kinematics. These variables could be expressed in terms of stiffness coefficients as: c_{33} , c_{55} , c_{66} , c_{11} and c_{13} (Figure 3.4).

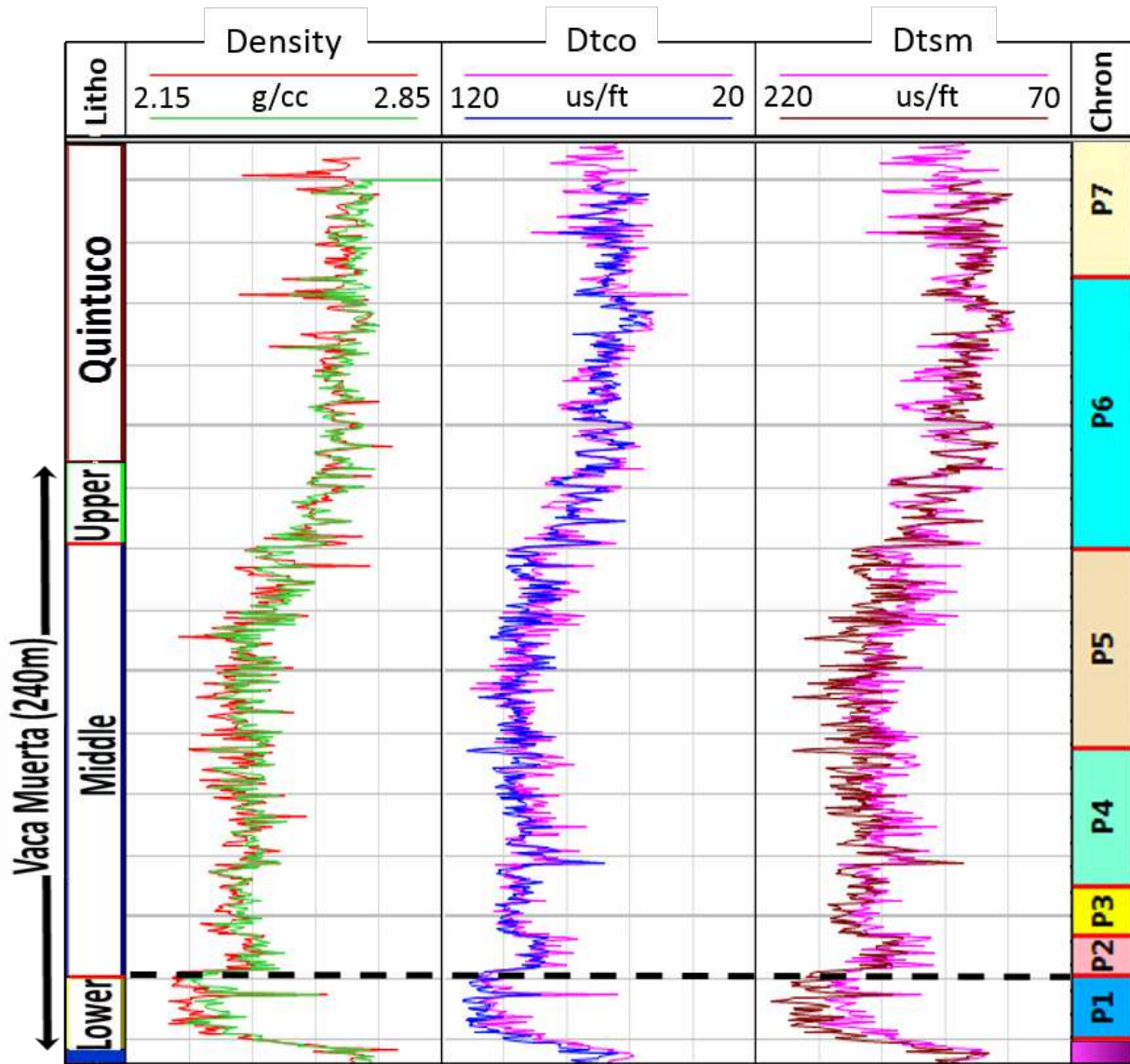


Figure 3.2: Comparison of acquired density and sonic logs with the results of the rock-physics model. Registered logs are shown in red (density) and pink color (sonics). Modeled curves are displayed in green (density), blue (compressional sonic) and magenta color (shear sonic). Lithostratigraphic tops are located on the leftmost track while parasequences (chronostratigraphic markers) are at the rightmost track.

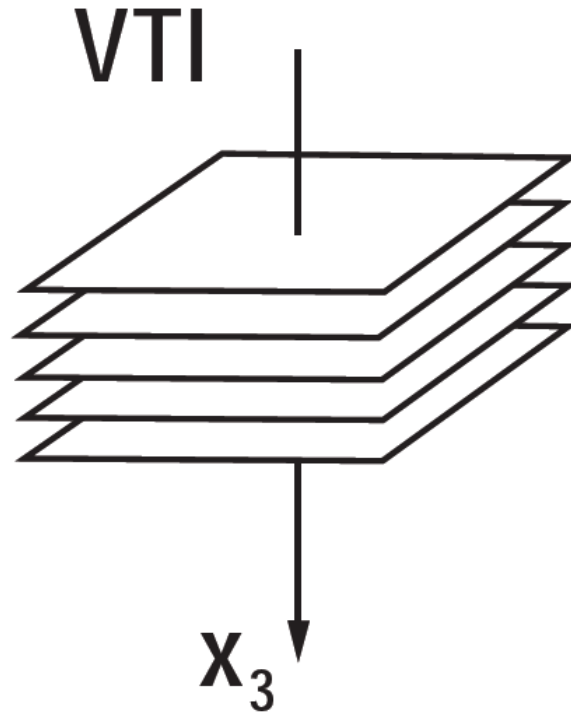


Figure 3.3: Schematic diagram of a VTI model. The vertical symmetry axis and horizontal isotropy planes can be seen. From Tsvankin (2012).

$$\mathbf{c}^{(\text{VTI})} = \begin{pmatrix} c_{11} & c_{11} - 2c_{66} & c_{13} & 0 & 0 & 0 \\ c_{11} - 2c_{66} & c_{11} & c_{13} & 0 & 0 & 0 \\ c_{13} & c_{13} & c_{33} & 0 & 0 & 0 \\ 0 & 0 & 0 & c_{55} & 0 & 0 \\ 0 & 0 & 0 & 0 & c_{55} & 0 \\ 0 & 0 & 0 & 0 & 0 & c_{66} \end{pmatrix}$$

Figure 3.4: Stiffness matrix of a VTI medium. From Tsvankin (2012).

Well logs may be used to calculate c_{33} and c_{55} using the vertical components of the compressional (V_p) and shear wave velocities (V_s) as follows:

$$c_{33} = \rho V_p^2 \quad \text{and} \quad c_{55} = \rho V_s^2 \quad (3.3)$$

The horizontal S_H -wave velocity (V_{S_H}) is needed to estimate c_{66} by implementing the relation below:

$$c_{66} = \rho V_{S_H}^2 \quad (3.4)$$

The horizontal S_H -wave velocity could be computed from Stoneley data, as it was described previously (section 3.2). Nevertheless, the quality of the Stoneley wave velocity depends on the borehole conditions, which may vary from well to well. For some wells of the study area Stoneley data weren't adequate to accurately calculate the horizontal S_H -wave velocity and obtain c_{66} .

Five independent parameters should be estimated to describe the velocity anisotropic response of the VM, but just two parameters can be computed for all study area wells, based on acquired logs. Core data were available yet three wells had them, Wells B, C and G. The parasequences described in chapter two were then integrated into the model building for data interpolation and extrapolation. Consequently, core data were grouped per parasequence to calculate the remaining stiffness coefficients.

Wintershall acquired cores of the VM section for Wells B, C and G. Analyzed samples were taken in vertical, horizontal and 45° orientation, at certain depths. Dynamic values of stiffness coefficients, anisotropic elastic moduli and Thomsen parameters were reported. Additionally, velocity measurements of P and S-waves at vertical, horizontal and 45° orientation were performed. Dynamic values of c_{33} , c_{55} , c_{66} , c_{11} and c_{13} were used for the anisotropic model building of the VM. Dynamic values of vertical and horizontal Young's modulus (E_{vert} and E_{hor}), and vertical-horizontal, horizontal and horizontal-vertical Poisson's ratio (ν_{vert} , ν_{horz} and $\nu_{horz-vert}$, respectively) were utilized as reference. Velocity measurements and dynamic Thomsen parameters were also used as reference.

Core data was grouped per parasequence and linear relationships were observed between dynamic values of stiffness coefficients measured on cores. Parameters of these linear relationships were estimated per parasequence. Parasequences were defined for all study area, where wells and/or seismic were existing. Then, parameters relating stiffness coefficients per parasequence allowed me to compute the remaining stiffness coefficients (c_{66} , c_{11} and c_{13}) where no core or other data were accessible.

Some linear relationships investigated between dynamic values of stiffness coefficients measured on cores were derived by Quirein et al. (2014) to properly model formations with a greater horizontal Poisson's ratio than the vertical counterpart. In addition, a linear relationship between horizontal and vertical Poisson's ratio should be observed. Core data of the VM showed a linear relationship between horizontal and vertical Poisson's ratio, being the horizontal Poisson's ratio larger than the vertical Poisson's ratio (Figure 3.5). Therefore, Quirein et al. (2014) empirical relations were valid to be applied on the VM to estimate c_{11} and c_{13} .

$$c_{11} = k_1(2(c_{66} - c_{55}) + c_{33}) \quad \text{and} \quad c_{13} = k_2 c_{12} \quad (3.5)$$

The other linear relationship implemented was derived by Murphy et al. (2015) to calculate c_{66} where no information of the horizontal S_H -wave velocity was available. This is the general case for the VM, as it was discussed previously in this section. The empirical relation found by Murphy et al. (2015) was based on the observed behavior of Thomsen parameters ϵ and γ , for several organic rich formations.

$$\epsilon = k_3 \gamma \quad \text{or} \quad \frac{c_{11} - c_{33}}{2c_{33}} = k_3 \frac{c_{66} - c_{55}}{2c_{55}} \quad (3.6)$$

The coefficients that define the two empirical relations mentioned above (k_1 , k_2 and k_3) should be computed for the formation to be modeled, in this case the VM, using core data. Core data were available just for Wells B, C and G. For this reason, parasequences were implemented to group core data and estimate k_1 , k_2 and k_3 per each parasequence (Figure 3.6). It allows to describe the five independent stiffness coefficients of a VTI model (c_{33} , c_{55} , c_{66} , c_{11} and c_{13}) volumetrically. The values of the coefficients (k_1 , k_2 and k_3) per parasequence can be seen in Figure 3.7.

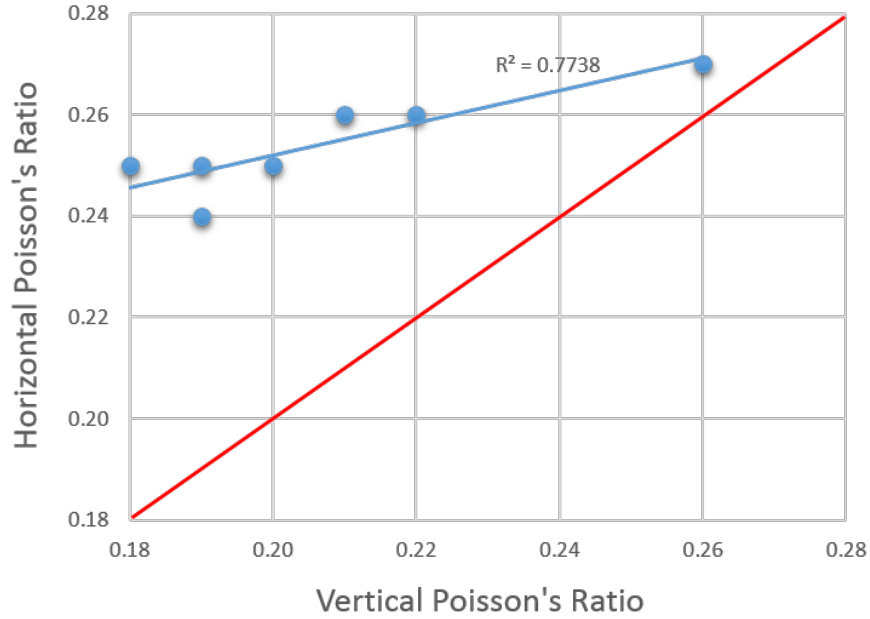


Figure 3.5: Crossplot of horizontal versus vertical Poisson's ratios. Dynamic moduli estimated on core for Well G. 1-1 line is shown in red.

Besides, values of k_1 , k_2 and k_3 estimated per parasequence may be classified by depositional facies. Interpreted slope and basin for the VM exhibited different behavior of dynamic stiffness coefficients (Figure 3.6).

In summary, the workflow to calculate the six stiffness coefficients, five independent, to fully describe the VTI model of the VM system is as follows:

1. c_{33} and c_{55} were obtained from equations 3.3
2. The expression for k_1 (Equation 3.5) and k_3 , written in function of stiffness coefficients (Equation 3.4), were integrated to solve for c_{66} (Equation 3.7)

$$c_{66} = \frac{2k_1 \frac{c_{55}}{c_{33}} + 1 - k_1 - k_3}{2k_1 \frac{1}{c_{33}} - k_3 \frac{1}{c_{55}}} \quad (3.7)$$

3. c_{11} was determined from k_1 relation (Equation 3.5)
4. c_{12} , the dependent parameter, was computed from the symmetry relation of a VTI model

$$c_{12} = c_{11} - 2c_{66} \quad (3.8)$$

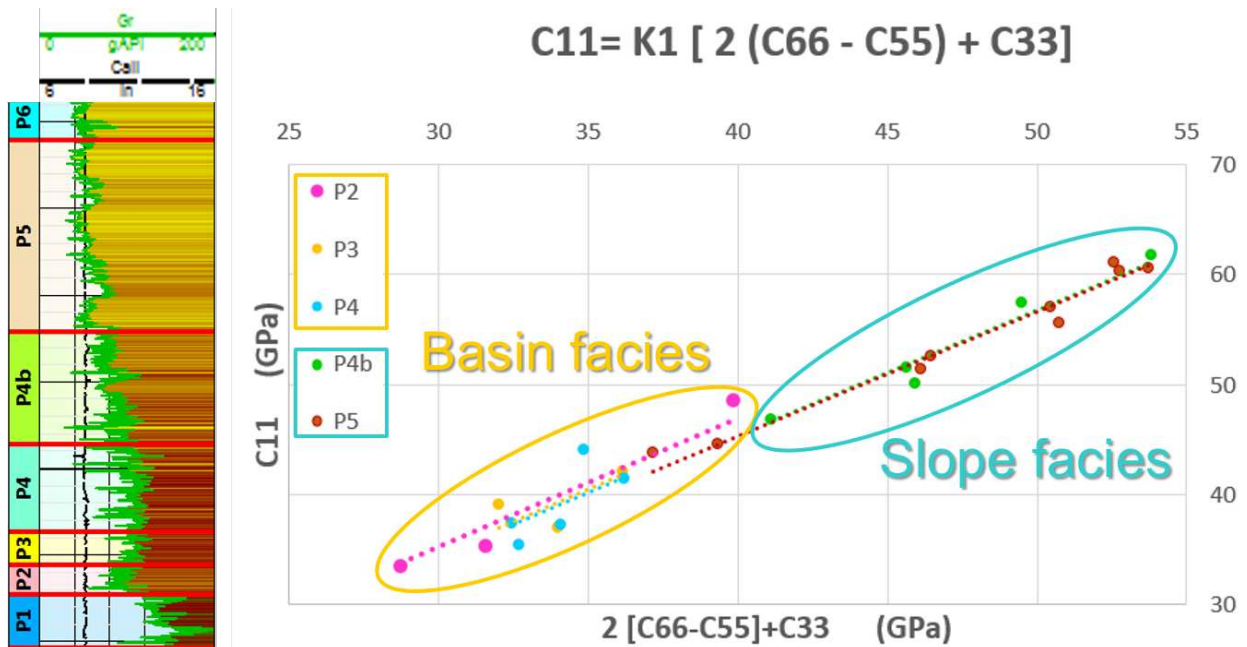


Figure 3.6: Crossplot of c_{11} versus $2(c_{66} - c_{55}) + c_{33}$ to estimate k_1 , per parasequence. GR and interpreted parasequences for Well G are shown at the left side. Parasequence could be grouped by their depositional facies. Behavior of interpreted slope and basin facies for the VM could be differentiated.

Parasequence	K1 (frac)	K2(frac)	K3 (frac)	# of samples
P1	1.149	0.894	1.234	Median of calculated values
P2	1.175	0.746	1.234	3
P3	1.157	0.894	1.372	3
P4	1.149	0.870	1.213	5
P4b	1.135	0.903	1.345	4
P5	1.134	0.899	1.214	8
P6	1.149	0.894	1.234	Median of calculated values
P7	1.149	0.894	1.234	Median of calculated values
P8	1.149	0.894	1.234	Median of calculated values
	1.149	0.894	1.234	Median-core data

Figure 3.7: k_1 , k_2 and k_3 coefficients calculated per parasequence.

5. And, c_{13} was estimated from the k_2 expression (Equation 3.6)

The use of well logs to compute c_{33} and c_{55} by implementing the equations 3.3 allowed me to obtain anisotropic elastic moduli for each well. Moreover, if inverted seismic cubes of vertical P and S_V -wave velocities are used, volumes of anisotropic elastic moduli may be generated for improved geomechanical models to be created.

Finally, anisotropic Young's modulus and Poisson's ratio were determined implementing the following equations:

$$E_{vert} = \frac{c_{33}(c_{11} + c_{12}) - 2c_{13}^2}{c_{11} + c_{12}} \quad E_{hor} = \frac{(c_{11} - c_{12})(c_{33}(c_{11} + c_{12}) - 2c_{13}^2)}{c_{11}c_{33} - c_{13}^2} \quad (3.9)$$

$$\nu_{vert} = \frac{c_{13}}{c_{11} + c_{12}} \quad \nu_{13} = \nu_{23} = \frac{c_{13}(c_{11} - c_{12})}{c_{33}c_{11} - c_{13}^2} \quad \nu_{12} = \nu_{21} = \frac{c_{33}c_{12} - c_{13}^2}{c_{33}c_{11} - c_{13}^2} \quad (3.10)$$

The methodology proposed to compute anisotropic elastic moduli was demonstrated for Well G since it has the richest dataset. Other approaches to estimate anisotropic elastic moduli will be covered. They were implemented to compare their results with the methodology proposed. Such analysis enabled me to validate the proposed methodology. The two additional models were based on dynamic Thomsen values determined on core, and k_1 , k_2 and k_3 coefficients computed per well, instead of per parasequence. For each technique, anisotropic elastic moduli and velocities were calculated for Well G. Velocities at vertical, horizontal and at 45° angle were determined by implementing the exact expressions derived by Tsvankin (1996). The models described and their results are presented below (Figure 3.8 and Figure 3.9):

1. Model built from dynamic Thomsen parameters measured on cores. Core data were grouped per parasequence to calculate the median value of Thomsen parameters Epsilon, Delta and Gamma, per each time-related package. Median values determined per parasequence were inverted to obtain c_{11} , c_{13} and c_{66} . Anisotropic elastic moduli and velocities were comparable to the values of the methodology proposed. However, it was observed that linear regressions, used for the methodology proposed, tied better to the core data than a median

approach, employed for the current model. This result was explained because linear regressions handle outliers better than median methodologies and the linear relationship depicted before between horizontal and vertical Poisson's ratio (Figure 3.5).

2. Model based on k_1 , k_2 and k_3 coefficients computed per well. c_{11} , c_{66} and c_{13} were derived per well applying the relations described before (Equation 3.5 and 3.6). This common procedure in industry is slightly different from the proposed methodology where k_1 , k_2 and k_3 coefficients were calculated per parasequence or depositional facies. Anisotropic elastic moduli and velocities were similar to the proposed methodology. The proposed methodology allowed for k_1 , k_2 and k_3 parameter variability along the well, defining a value per each parasequence. Besides, the proposed model allows for an approximation of the anisotropic elastic moduli response in wells without core data where parasequences were defined.

Differences observed between log and core velocities may be explained by the frequency of the measurement (Figure 3.9). Core velocity values are acquired at higher frequencies than velocity values of well logs. Velocity values measured on core are larger than those of logs. P-wave log velocity was modeled at high frequencies (core) by implementing the expression of Geertsma and Smit (1961). It enabled me to explain differences between log and core velocities due to frequency dispersion. It allowed me to represent viscous and inertial interactions between pore fluid and matrix minerals of the reservoir. The required inputs were the bulk modulus and density of the matrix (K_0 , ρ_0), fluid (K_{fl} , ρ_{fl}) and frame (K_{fr} , ρ_{fr}), and the tortuosity of the system (α) (Figure 3.10).

The mixed matrix described for the rock-physics modeling (section 3.2) was used to obtain bulk modulus and density of the matrix. The acoustic properties of the fluids determined by the mentioned rock-physics model were also implemented to get bulk modulus and density of the fluids, in this case oil and water. No fluid substitution was applied since there is no invasion in unconventional reservoirs. Then, frame bulk modulus and density were directly calculated from sonic and density well logs. Also, a high tortuosity value of three was assigned, assuming pores

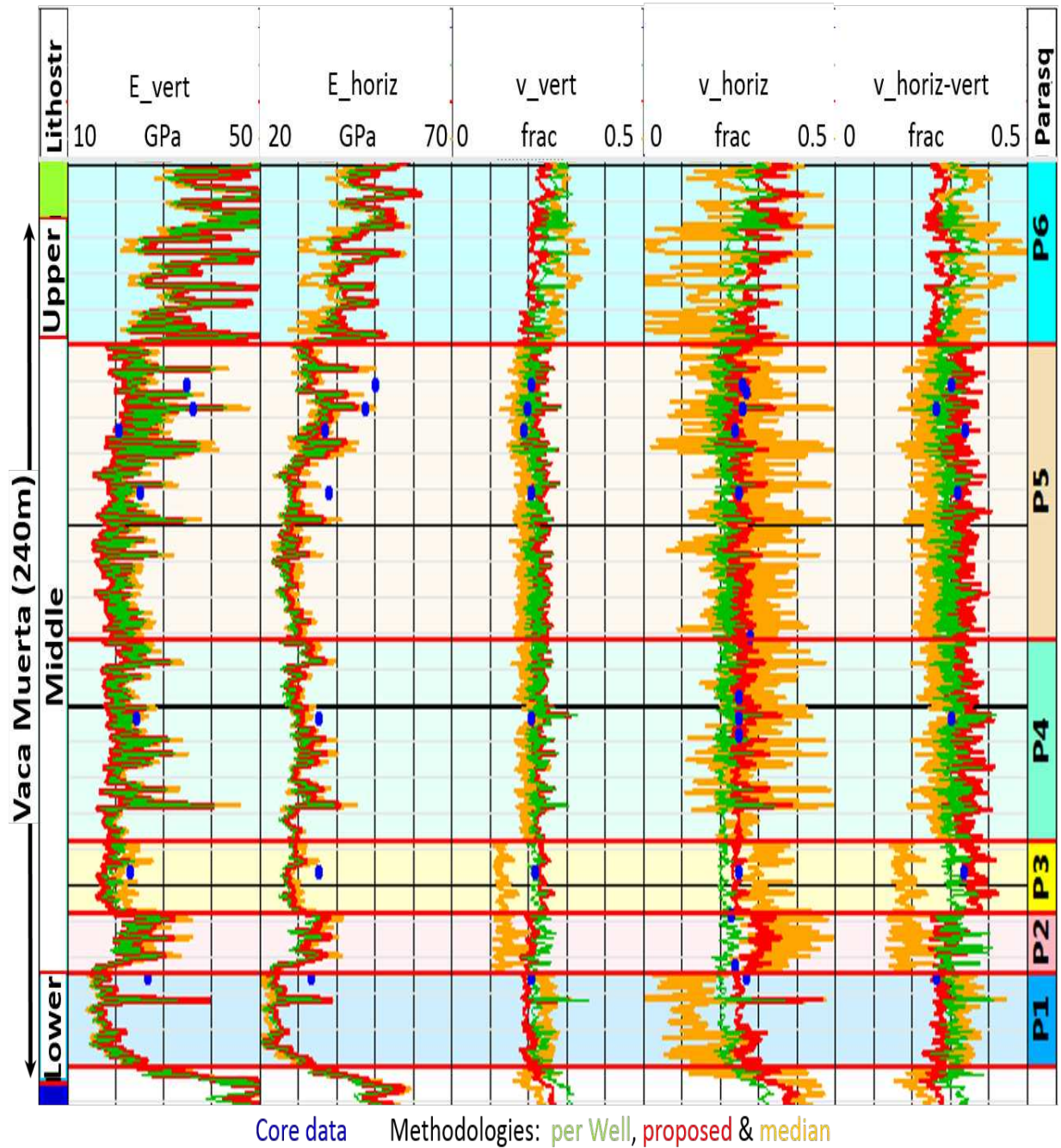


Figure 3.8: Comparison of anisotropic elastic moduli derived according to the described methodologies for Well G. Orange curves were obtained from median of dynamic Thomsen core values per parasequence, red logs from the proposed methodology, green curves from the common practice of computing k_1 , k_2 and k_3 coefficients per well, and blue-colored circles correspond with the dynamic core measurements of anisotropic elastic moduli.

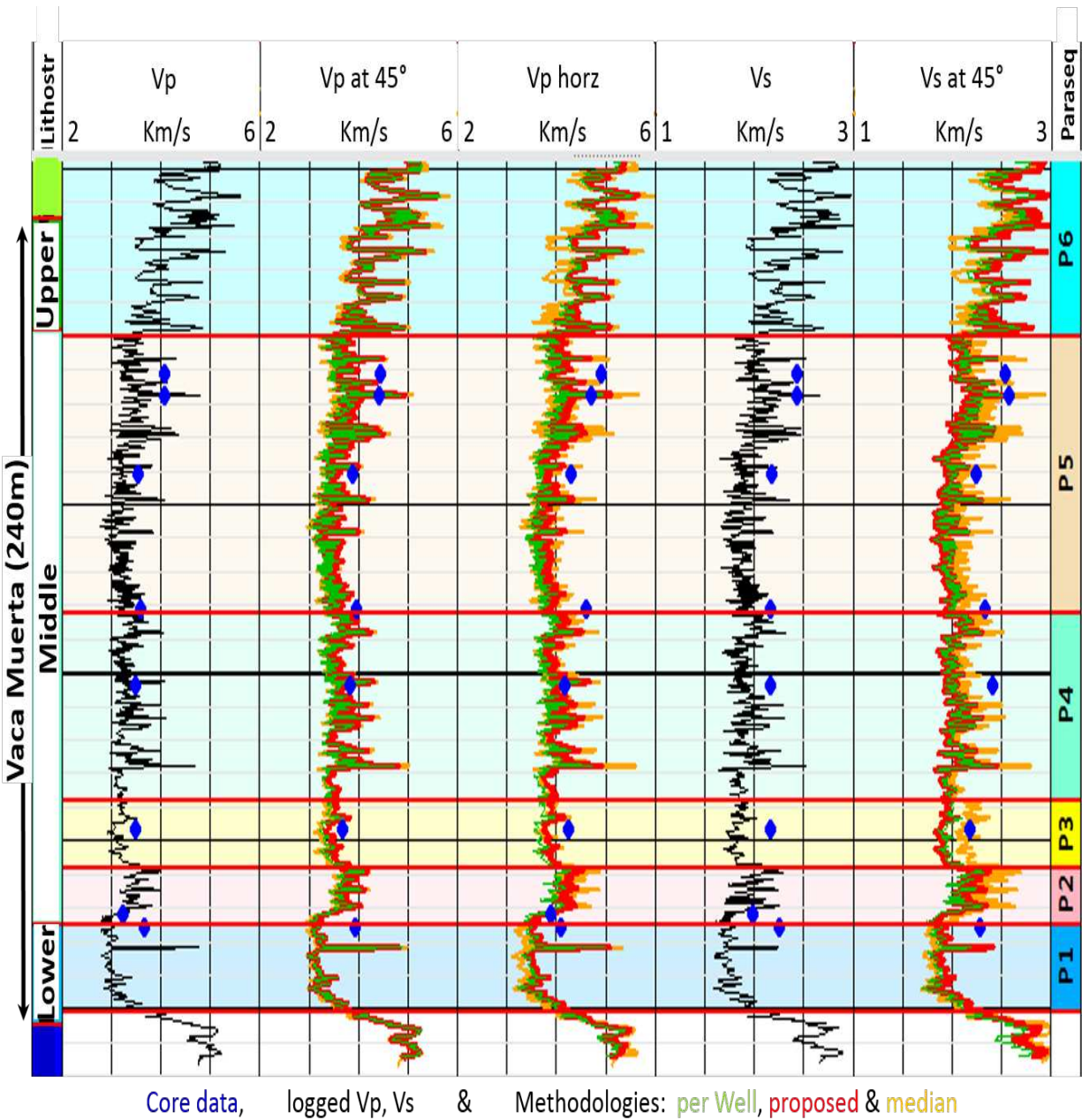


Figure 3.9: Velocity comparison of Compressional and Shear waves derived from the described methodologies for Well G. Orange curves were obtained from median of dynamic Thomsen core values per parasequence, red logs from the proposed methodology, green curves from the common practice of computing k_1 , k_2 and k_3 coefficients per well, and blue-colored circles correspond with the velocities measured in core. Logged vertical V_p and V_s are shown in black color.

$$V_{P\infty} = \left\{ \frac{1}{\rho_0(1 - \phi) + \phi\rho_{fl}(1 - \alpha^{-1})} \left[(K_{fr} + \frac{4}{3}\mu_{fr}) + \frac{\phi \frac{\rho}{\rho_{fl}} \alpha^{-1} + \left(1 - \frac{K_{fr}}{K_0}\right) \left(1 - \frac{K_{fr}}{K_0} - 2\phi\alpha^{-1}\right)}{\left(1 - \frac{K_{fr}}{K_0} - \phi\right) \frac{1}{K_0} + \frac{\phi}{K_{fl}}} \right] \right\}^{1/2}$$

Figure 3.10: Approximation of the P-wave velocity at the frequency of the core (Geertsma and Smit, 1961).

were randomly oriented, since the VM is a shale oil reservoir. Sensitivity of this parameter could be interesting topic to investigate. Interpreted depositional facies for the VM could contribute in that direction. As a result, P-wave velocity at core frequency was obtained.

Differences between logged and modeled P-wave velocities at high frequencies had the tendency to increase with depth. Modeled P-wave velocity at high frequencies tied better core data than P-wave standard sonic log velocity (Figure 3.11). It demonstrated that velocity differences between log and core for the VM could be explained in terms of the frequency of the measurement. The expression used to model P-wave log velocity at core frequencies is an isotropic relation. The anisotropic form of Gassmann's equation will be worth investigating to understand differences between velocities in core and well logs due to the frequency of the measurement, accounting for velocity anisotropy.

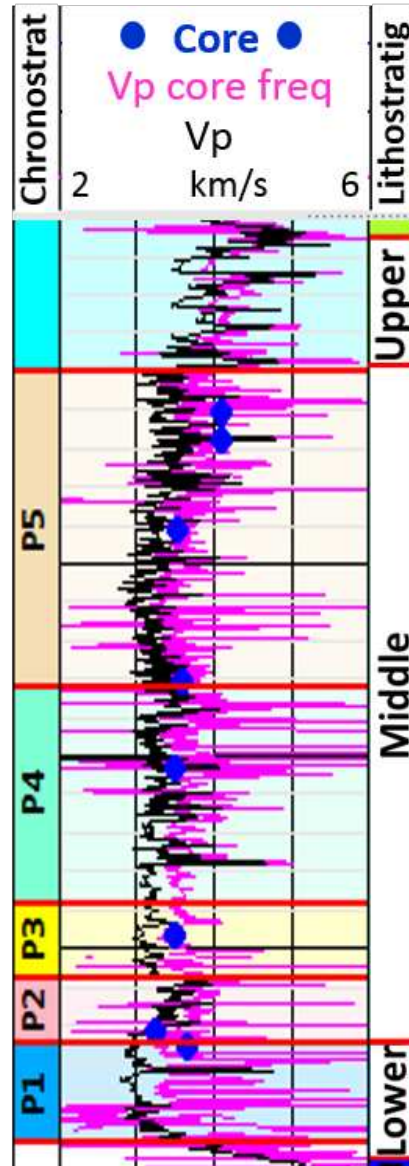


Figure 3.11: P-wave velocity modeled at high frequencies by implementing the Geertsma and Smit (1961) approximation, for Well G. V_p from the sonic well log is shown with the black curve, modeled V_p at the infinite frequency is displayed in pink, and core data is exhibited with blue-colored circles.

CHAPTER 4

INTEGRATED INTERPRETATION

This chapter will address the value of obtaining anisotropic elastic moduli and their control on stimulation and production of the VM. The benefit of determining anisotropic elastic moduli for the generation of geomechanical models may lead to more efficient drilling, completion and stimulation.

Anisotropic Young's modulus and Poisson's ratio were compared with the isotropic moduli and dynamic core data to assess the importance of anisotropic estimations (Figure 4.1). Accounting for anisotropy of the VTI medium yielded three additional moduli: Horizontal Young's modulus (E_{hor}), horizontal Poisson's ratio (ν_{horz}) and horizontal-vertical Poisson's ratio ($\nu_{horz-vert}$).

Horizontal Young's modulus was up to 25% higher than the isotropic modulus. Horizontal-vertical Poisson's ratio presented the largest deviation from the isotropic Poisson's ratio. Anisotropic determinations are believed to provide more accurate inputs for geomechanical models than isotropic moduli. In addition, they lead to better estimations of stress state of the VM, which will directly impact the design of well-related operations.

Poisson's ratios obtained by accounting for anisotropy - ν_{horz} and $\nu_{horz-vert}$ - described the strain response of the reservoir when stress is applied horizontally, which is the case for hydraulic fracturing in Well G, for example. The horizontal Poisson's ratio illustrates the ratio between horizontal strains, which may be understood as the rock is prone to fail in the horizontal direction (Figure 4.2). The horizontal-vertical Poisson's ratio is the fraction of the vertical over the horizontal strain. Small values indicate that the rock is prone to develop a vertical fracture width (Figure 4.3). As a result, E_{hor} , ν_{horz} and $\nu_{horz-vert}$ were mainly used for the integrated analysis presented below.

Previous to the integration of other datasets it is important to mention that Well G was completed in four stages within the VM. They were numbered in ascending order from the base to the top of the VM. Stages one and two corresponded to basin floor facies; while stages three and four

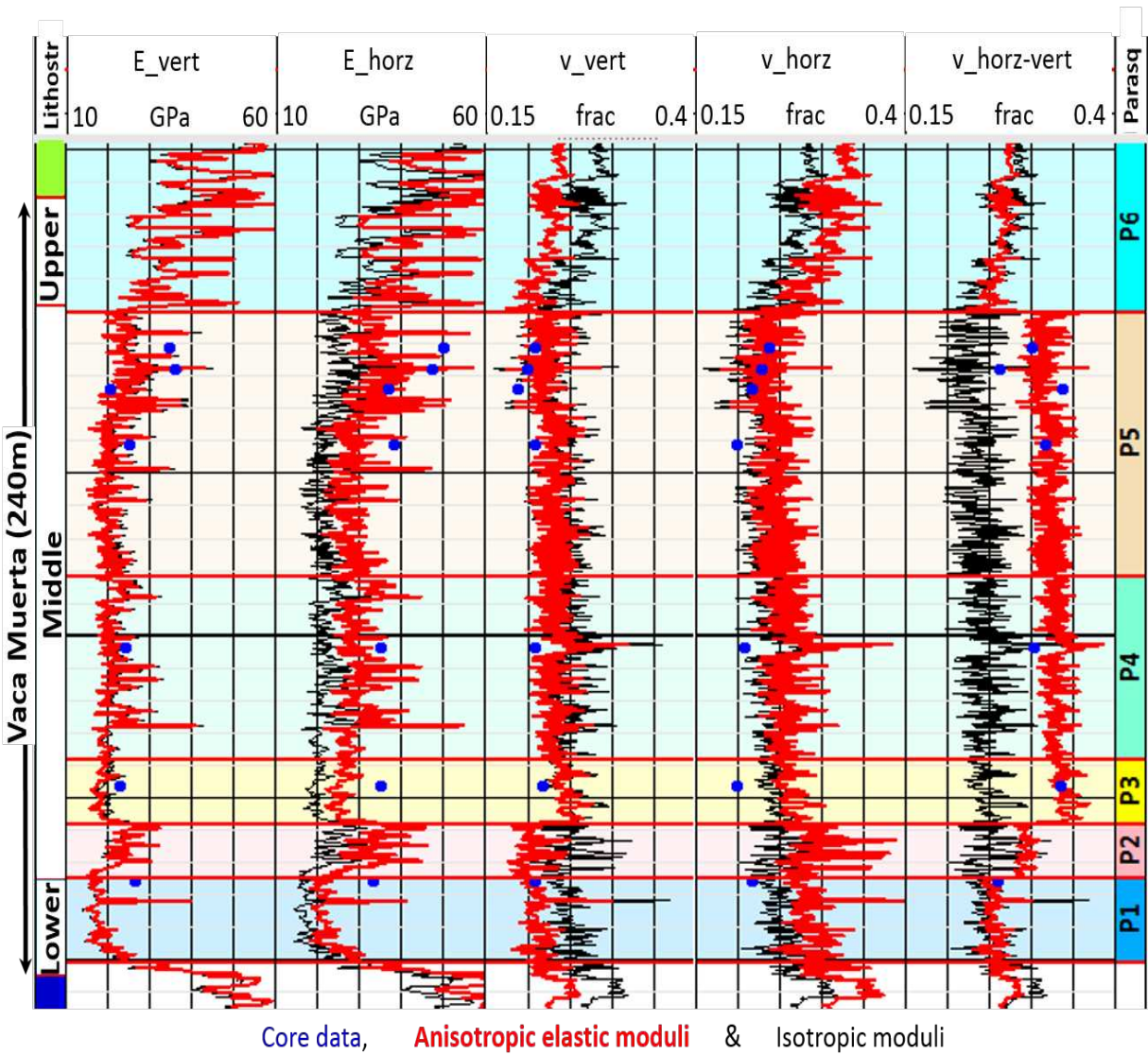


Figure 4.1: Comparison of isotropic with anisotropic elastic moduli for Well G. Isotropic moduli are shown with the black-colored lines, anisotropic with the red lines and dynamic core data are displayed with blue-colored circles.

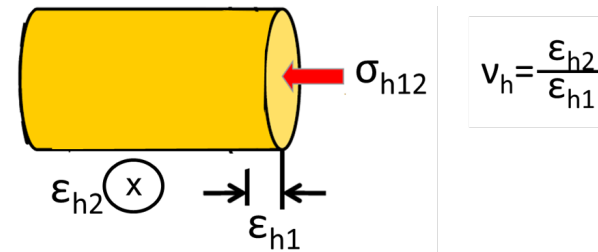


Figure 4.2: Schematic representation of horizontal Poisson's ratio (ν_{horz}). Modified from Bratton (2014).

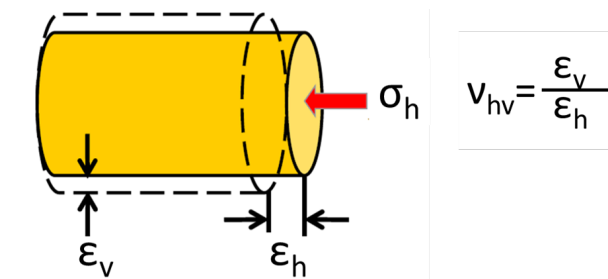


Figure 4.3: Schematic representation of horizontal-vertical Poisson's ratio ($\nu_{horz-vert}$). Modified from Bratton (2014).

were located in the slope facies of the depositional system. Figure 4.4 shows the amount of perforations per stage, the pressure range during the hydraulic fracturing and the normalized proppant injected volume.

Stage	Number of perforations	Relative pressure range (psi)	Relative CI volume
1	3	600-5100	0.46
2	4	800-4500	0.72
3	3	700-5400	0.72
4	7	300-5200	1

Figure 4.4: Completion information for Well G. Relative completed injected (CI) volume per stage is shown. Modified from White (2016).

The first piece of information that was investigated with the anisotropic elastic moduli was the dipole sonic log run before and after the hydraulic fracturing of Well G. Slow vertical S-wave slowness after and before the well stimulation were subtracted and the curve was displayed twice, with normal and reserve scale. Therefore, a slow shear-based anisotropy log was generated to assess the efficiency of the stimulation job (Figure 4.5, second track from right to left). Immediately, two different signatures were spotted in the slow shear-based anisotropy log. One corresponding to small values of the log, which were also depth-localized and the other exhibiting large and depth-continuous values. The first pattern was identified for the middle section of the VM, stages two and three, where natural fractures were interpreted by Bishop (2015). The stimulation has reactivated pre-existing fracture sets and fracture reorientation has occurred (Figure 4.6). Note that the fractures may not have been tectonic fractures. At the top and base of the VM, stages four and one, where no natural fractures were identified, the stimulation was not controlled by pre-existing fracture sets. The stimulation parameters were different between stages (Figure 4.4). Stage four had twice as many perforations as other stages. Thus, more proppant was injected, enabling an increased induced vertical fracture growth, which also explained the large values of slow shear-based anisotropy evidenced.

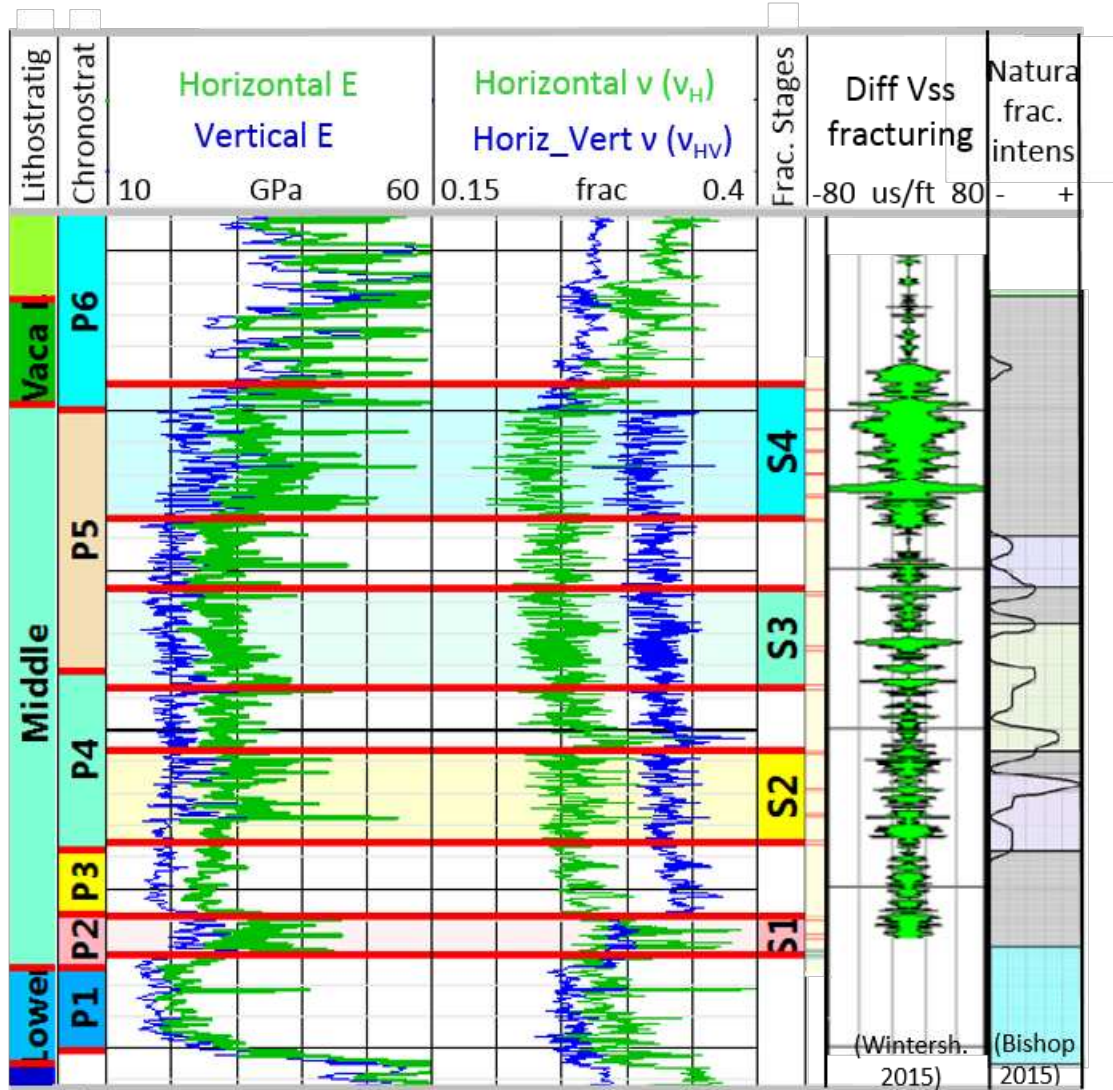


Figure 4.5: Integration of anisotropic elastic moduli with dipole sonic response and natural fractures intensity logs for Well G. The slow shear-based anisotropy log derived from the dipole sonic is displayed in the second track from right to left. A natural fracture intensity log generated by Bishop (2015) is exhibited at the rightmost track. Completed stages, chronostratigraphic and lithostratigraphic tops are also shown.

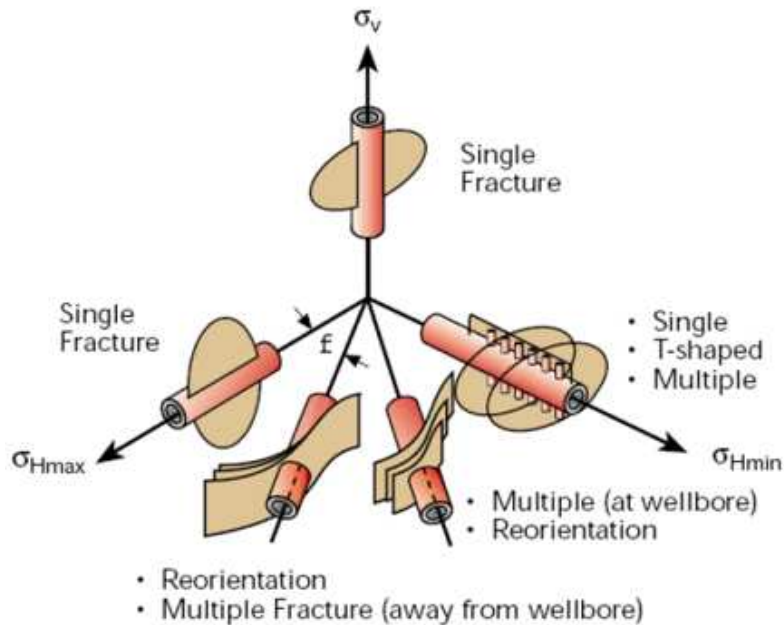


Figure 4.6: Simplified illustration of induced fracture geometries depending on borehole and stress orientations (Barree & Associates).

The response of the stimulation was analyzed according to data from the dipole sonic and the computed anisotropic elastic moduli. Microseismic data were integrated to obtain more information to characterize the VM. Few events were recorded for all the completed stages and the largest number of microseismic events were located above stage four. Two main focal mechanisms were interpreted: left strike-slip (Figure 4.7, magenta beach ball diagrams) and right oblique-slip (Figure 4.7, light blue beach ball diagrams). The first one could be explained by the present maximum horizontal stress (E-W) while the right oblique-slip could be correlated with a former stress state (NW-SE). These events were localized in the VM and Quintuco Formations, respectively. It should be mentioned that natural fractures sets with similar orientations to the ones present in the middle section of the VM were identified for the Quintuco Formation, but in a larger amount. In addition, Figure 4.7 reveals that left strike-slip events were aligned while right oblique-slip events appeared in clusters.

With the stimulation response investigated, production data will be evaluated. Two production logging tools (PLTs) were acquired in Well G. One in October, 2015 and other in May, 2016.

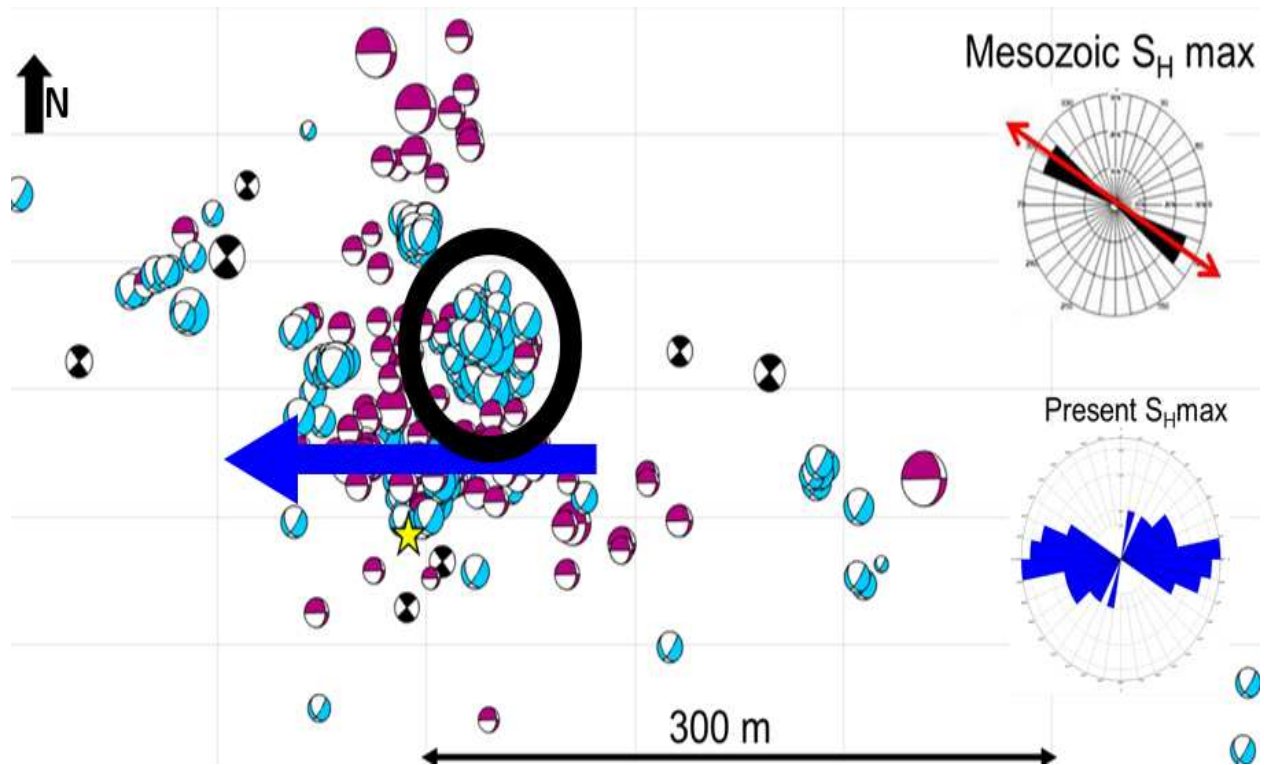


Figure 4.7: Map display of microseismic events with focal mechanisms and correlated stress states for Well G. Induced fractures correspond to left strike-slip events (magenta beach ball diagrams). They correlate with present maximum horizontal stress; while natural fractures depicted with right oblique-slip mechanisms (light blue beach ball diagrams) have a relationship with former maximum horizontal stress. Modified from White (2016).

Temperature differentials were used to compare production over time. Flow rates exhibited higher uncertainty for this dataset. Flow rates were under tool resolution for the first PLT. The response of the two PLTs is very similar. This is an important piece of information as it demonstrates that contributions per stage did not change during the seven month period. Forty to fifty percent of the oil production of this well came from stage four. Whereas, stages one, two and three contributed with the remaining sixty to fifty percent, having a very similar performance (Figure 4.8).

Other rock properties were brought into this study to provide a more complete picture of the VM mechanical behavior. Properties including mineral fractions, porosity, TOC and oil saturation were included. Mineral fractions, total porosity and oil saturation came from the petrophysical evaluation performed at Wintershall by Pablo Pateti, in August 2016. TOC was evaluated from litho-scanner tool response, which was in agreement with the Schmoker empirical equation and core tests as it was shown in chapter two (Figure 4.8).

Clay content was very stable for the VM. Calcite and silicates fractions had opposite behaviors. In general, calcite content was increasing towards the top of the VM whereas silicates increased towards the base. No correlations were identified between relative high amounts of calcite and/or silicates and large oil productions. The same statement held for the total porosity.

A detailed analysis of the isochron of parasequences 4b to 5 revealed that Well G was located at the slope toe areas of the basin for the time the VM was deposited (Figure 2.11). There, the environment had less oxygen and allowed for high concentrations of TOC, as the litho-scanner evidenced.

As expected, oil saturation impacted interval performance as the case for stage four with the largest oil saturation and the highest oil production. Conversely, intervals with relative low TOC within the VM were more productive than sections with high TOC. Such behavior was due to the direct relation between rock compliance and kerogen amount. Fracture containment also played a role. Brittle reservoir intervals bounded by ductile rock packages (higher TOC values) develop contained fractures, when they are stimulated. It was shown in Chapter two that TOC can be determined from acoustic impedance by implementing a linear regression. Then, TOC volumes could

be used to assess intervals that may act as containment intervals during the hydraulic fracturing process.

My integrated interpretation is summarized as follows:

1. Induced fractures (E-W) were created by the stimulation process where natural fractures weren't interpreted on image logs (stages one and four, Lower and Upper VM). They were correlated with the left strike-slip focal mechanisms described, which are aligned in map and depth view. Such behavior is recognized with the fracture modeling of the completed intervals where the model demonstrated that stages one and four have long fracture lengths (Personal communication with Wintershall's reservoir engineer, Hernan Bujis, in 2016).
2. Natural fractures (NW-SE) were primarily reactivated by the hydraulic fracturing operation of stages two and three (located in the Middle VM). Moreover, pre-existing fracture sets identified in the Quintuco Formation were also accessed by stage four. Right oblique-slip focal mechanisms depicted by microseismic relate to a previous stress state in agreement with the orientation of these planes of weakness. Contrary to induced fracture sets, natural fractures denote a cluster occurrence in map and depth view which produce small fracture lengths. Fracture modeling also revealed a higher permeability of the system for stage three which can be explained by the presence of natural fractures (Personal communication with Wintershall's reservoir engineer, Hernan Bujis, in 2016).
3. Induced and natural fractures exhibit distinct characteristics in terms of location, orientation, areal and depth behavior. They impact well-related operations. For instance, wellbores and well completions should be oriented consistently with pre-existing fracture sets and the current stress state to maximize the efficiency of stimulation jobs. Likewise, optimum well spacing will differ depending on the targeted interval and its probability to develop induced or reactivate natural fractures.
4. Stage four is the largest oil producer. It accounts for around 40% of the oil production. While, stages one, two and three produced almost the same. The production mechanisms

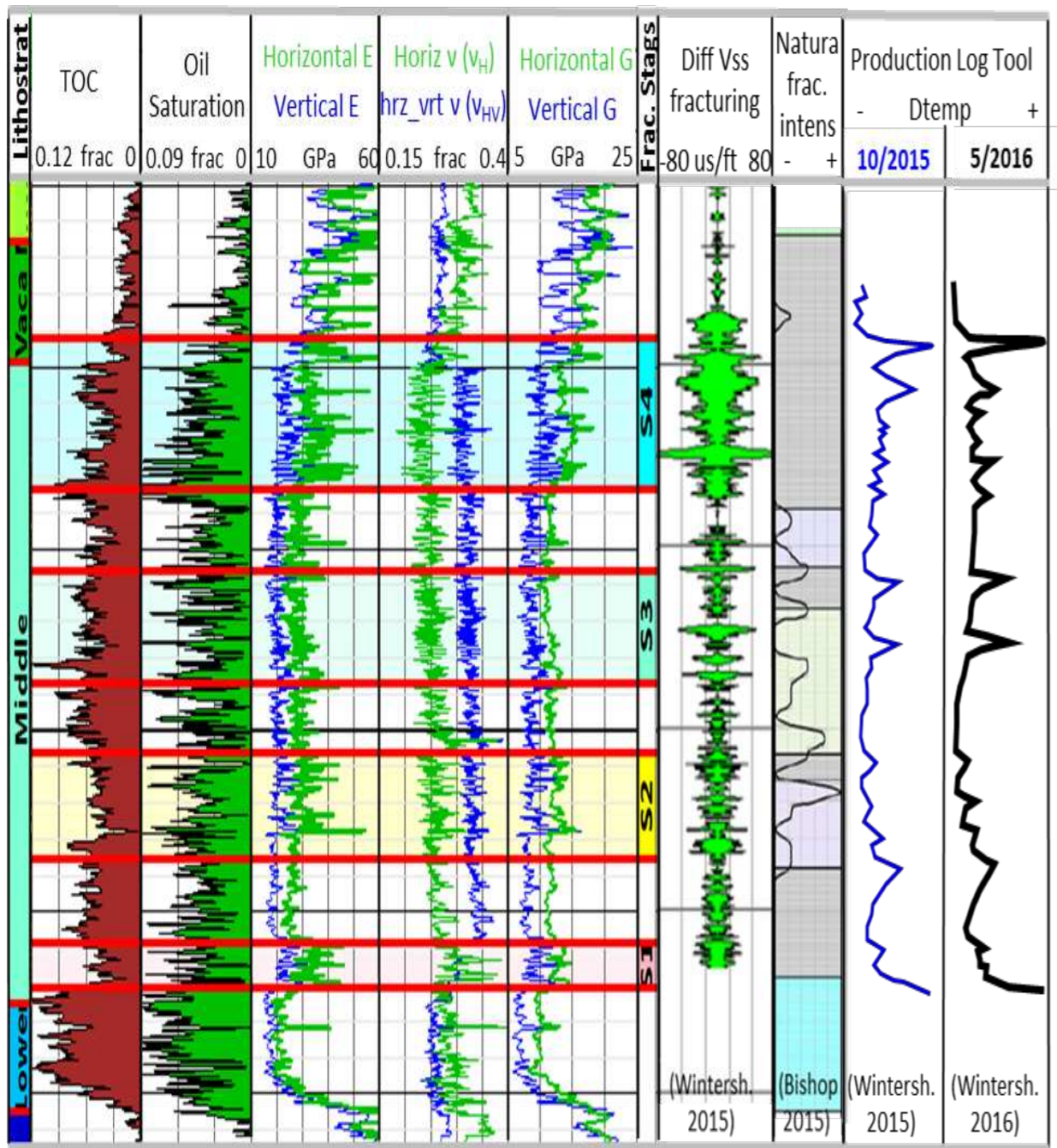


Figure 4.8: Integration of anisotropic elastic moduli with rock properties, stimulation and production tools for Well G. From left to right are displayed, lithostratigraphic tops, TOC, oil saturation, anisotropic elastic moduli, completed stages, the slow shear-based anisotropy log derived from the dipole sonic, natural fractures intensity log and the acquired PLTs.

interpreted for each stages were different. Stages four and ones were producing by the creation of induced fractures. Nevertheless, increased production in stage four could be due to a connection of the VM with the Quintuco Formation, which is a naturally fracture reservoir. Stage one is proximal to the richest source rock of the VM. Stages two and three produce from the reactivation of natural fractures. Stage three was deposited in the slope of the system while stage two was in the basin floor facies. Stage three evidenced higher permeability and slightly higher production than two. Internal characteristics of the completed interval three, related with its depositional environment, could have an impact on an increased production for this stage. Such behavior should be analyzed further by a detailed facies study of the VM.

This study propose a methodology to estimate anisotropic elastic moduli for better describing the behavior of the VM to well stimulation. They provide more accurate inputs to perform estimations of stress state as input to geomechanical modeling. Anisotropic moduli enable the selection of zones that will perform better under hydraulic fracture stimulation giving rise to better economic decisions for the development of the VM.

CHAPTER 5

CONCLUSIONS

From this study the following conclusions are drawn:

1. Using a sequence stratigraphic approach and seismic stratigraphy I identified parasequences in the Vaca Muerta Formation (VM). They helped me distinguish two depositional environments in the VM with unique characteristics. A petrophysical evaluation tied with seismic data allowed me to identify basin floor and slope facies. Rock properties varied according to depositional facies. This knowledge should be included in the design of drilling and completion well-operations.
2. Parasequence definition enabled me to build an anisotropic model for the VM. Parasequences were used to group and interpolate core and well log data to compute anisotropic elastic moduli. In a similar way parasequences can be applied for the generation of depositional-driven low-frequency models to perform inversions of available seismic data to predict rock properties.
3. Acoustic impedance in the VM exhibited an inverse relationship with the TOC (The acoustic impedance decreases, TOC increases). Hence, TOC can be estimated from inverted seismic volumes of acoustic impedance. TOC cubes are important for unconventional sweet spot definition since TOC correlates with porosity and hydrocarbon saturation and contributes to identification of zones with large hydrocarbon pore volume.
4. Anisotropic elastic moduli were computed assuming that VM has a VTI symmetry. Anisotropic elastic moduli provide a better input to geomechanical modeling than isotropic moduli. In addition, the spatial variations of anisotropic elastic moduli could guide identification of preferable zones for hydraulic fracturing.

5.1 Future work

Future work is recommended including:

1. Use of the anisotropic form of Gassmann's equation to model velocity response at low frequencies. This approach will allow one to determine the differences between velocities in core and well logs due to the frequency of the measurement.
2. Create rock-physics models to analyze the sensitivity of parameters like, lithology, porosity, TOC, saturation, pore pressure, fracture presence and geometry on velocities and densities of the VM. It will provide information about causes of anisotropy at well log and core data scale. They will enable the computation of rock properties from impedances and/or velocity and density volumes. Such knowledge will generate value for sweet spot definition of the VM and design of well-related operations.
3. Incorporate uncertainty analysis and blind tests to the methodology proposed. Several scenarios for stress state and geomechanical models can be built based on the range of possible values of anisotropic elastic moduli. As more core data becomes accessible, the accuracy of the model to predict the elastic moduli could be investigated.
4. Integrate future multicomponent seismic data to the methodology I have created from mainly core and log analysis. It will allow for more robust determination of anisotropic elastic moduli for improved geomechanical modeling of the VM.

REFERENCES CITED

- Askenazi, A., P. Biscayart, M. Cáneva, and S. Montenegro (2013), Analogía entre la Formación Vaca Muerta y Shale Gas / Oil Plays de EEUU, *Society of petroleum engineers*, p. 20.
- Batzle, M., and Z. Wang (1992), Seismic properties of pore fluids, *Geophysics*, 57(11), 1396 – 1408, doi:10.1190/1.1443207.
- Bishop, K. (2015), Mechanical Stratigraphy of the Vaca Muerta Formation, Neuquen Basin, Argentina, Master of science degree, Colorado School of Mines.
- Bratton, T. (2014), Well Log Analysis and Formation Evaluation.
- EIA, U. S. (2013), Technically Recoverable Shale Oil and Shale Gas Resources: An Assessment of 137 Shale Formations in 41 Countries Outside the United States, *Tech. rep.*, US Energy Information Administration (EIA), Washington, D. C.
- Embry, A. (2009), *Practical Sequence Stratigraphy*, online ed., 81 pp., Canadian Society of Petroleum Geologists, Canada.
- Fernandez Badessich, M., D. Hryb, M. Suarez, L. Mosse, N. Palermo, S. Pichon, and L. Reynolds (2016), Vaca Muerta Shale-Taming a Giant, *Oilfield Review*, January(1), 14.
- Fernandez-Concheso M., J. E. (2015), Characterizing an Unconventional Reservoir With Conventional Seismic Data: a Case Study Using Seismic Inversion for the Vaca Muerta Formation, Neuquen Basin, Argentina, Master of science degree, Colorado School of Mines.
- Gani, M. R., and J. P. Bhattacharya (2005), Lithostratigraphy versus chronostratigraphy in facies correlations of Quaternary deltas: Application of bedding correlation, in *River deltas: Concepts, models, and examples*, pp. 31–48, SEPM Special Publication 83.
- Garcia, M. N., F. Sorenson, J. C. Bonapace, F. Motta, C. Bajuk, and H. Stockman (2013), Vaca Muerta Shale Reservoir Characterization and Description: The Starting Point for Development of a Shale Play with Very Good Possibilities for a Successful Project, in *Unconventional Resources Technology Conference (URTeC)*, Society of Petroleum Engineers, Denver, Colorado, USA, doi:10.1190/urtec2013-090.
- Geertsma, J., and D. C. Smit (1961), SOME ASPECTS OF ELASTIC WAVE PROPAGATION IN FLUID-SATURATED POROUS SOLIDS, *Geophysics*, XXVI(2), 169–181.

- Han, D. (1987), Effects of porosity and clay content on acoustic properties of sandstones and unconsolidated sediments, Ph.d, Stanford University, doi:5477973.
- Howell, J. A., E. Schwarz, L. A. Spalletti, and G. D. Veiga (2005), The Neuquen Basin: an overview, *Special Publications. Geological Society*, 252, 1–14.
- Kietzmann, D. A., R. M. Palma, A. C. Riccardi, J. Martin-Chivelet, and J. Lopez-Gomez (2014), Sedimentology and sequence stratigraphy of a Tithonian-Valanginian carbonate ramp (Vaca Muerta Formation): A misunderstood exceptional source rock in the Southern Mendoza area of the Neuquén Basin, Argentina, *Sedimentary Geology*, 302, 64–86, doi:10.1016/j.sedgeo.2014.01.002.
- Legarreta, L., and H. J. Villar (2011), Geological and Geochemical Keys of the Potential Shale Resources, Argentina Basins, *Geoscience Technology Workshop Unconventional Resources: Basics, Challenges, and Opportunities for New Frontier Plays*, 80196(1), 28.
- Legarreta, L., H. J. Villar, G. A. Laffitte, C. E. Cruz, and G. Vergani (2005), Cuenca Neuquina: Balance De Masa Enfocado a La Evaluacion Del Potencial Y De Las Zonas No Productivas, in *VI Congreso de Exploración y Desarrollo de Hidrocarburos*, pp. 233–250, Mar del Plata, Argentina.
- Mosquera, A., and V. A. Ramos (2006), Intraplate deformation in the Neuquén Embayment, *Special Paper. Geological Society of America*, 407(05), 97–123, doi:10.1130/2006.2407(05).
- Murphy, E., S. R. Barraza, M. Gu, D. Gokaraju, M. E. Far, and J. Quirein (2015), New Models for Acoustic Anisotropic Interpretation in Shale, in *SPWLA Annual Logging Symposium*, Society of Petrophysicists and Well Log Analysts (SPWLA), Long Beach, California, USA.
- Passey, Q. R., S. Creaney, J. B. Kulla, F. J. Moretti, and J. D. Stroud (1990), Practical model for organic richness from porosity and resistivity logs, *American Association of Petroleum Geologists Bulletin*, 74(12), 1777–1794, doi:10.1306/OC9B25C9-1710-11D7-8645000102C1865D.
- Quirein, J., M. Eid, and A. Cheng (2014), PREDICTING THE STIFFNESS TENSOR OF A TRANSVERSELY ISOTROPIC MEDIUM WHEN THE VERTICAL POISSON ' S RATIO IS LESS THAN THE HORIZONTAL POISSON ' S RATIO, in *SPWLA Annual Logging Symposium*, pp. 1–11, Society of Petrophysicists and Well Log Analysts (SPWLA), Abu Dhabi, United Arab Emirates.
- Rodrigues, N., P. R. Cobbold, H. Loseth, and G. Ruffet (2009a), Widespread bedding-parallel veins of fibrous calcite ('beef') in a mature source rock (Vaca Muerta Fm, Neuquén Basin, Argentina): evidence for overpressure and horizontal compression, *Journal of the Geological Society*, 166(4), 695–709.

- Rodrigues, N., P. R. Cobbold, H. Loseth, and G. Ruffet (2009b), Widespread bedding-parallel veins of fibrous calcite ('beef') in a mature source rock (Vaca Muerta Fm, Neuquén Basin, Argentina): evidence for overpressure and horizontal compression, *Journal of the Geological Society*, 166(July), 695–709, doi:10.1144/0016-76492008-111.
- Sagasti, G., A. Ortiz, D. Hryb, M. Foster, and V. Lazzari (2014), Understanding Geological Heterogeneity to Customize Field Development: An Example From the Vaca Muerta Unconventional Play, Argentina, in *Unconventional Resources Technology Conference (URTeC)*, Society of Petroleum Engineers, Denver, Colorado, USA, doi:10.15530/urtec-2014-1923357.
- Schmoker, J. W. (1979), Determination of organic content of Appalachian Devonian shales from formation-density logs., *American Association of Petroleum Geologists Bulletin*, 63(9), 1504–1509, doi:10.1306/2F9185D1-16CE-11D7-8645000102C1865D.
- Stinco, L. P. U. d. B. A., and S. I. T. d. B. A. Barredo (2014), Vaca Muerta Formation: An Example of Shale Heterogeneities Controlling Hydrocarbon Accumulations, in *Unconventional Resources Technology Conference (URTeC)*, p. 15, Society of Petroleum Engineers, Denver, Colorado, USA, doi:10.15530/urtec-2014-1922563.
- Tosaya, C. A. (1982), Acoustical properties of clay-dearing rocks., Ph. d., Stanford University.
- Tsvankin, I. (1996), P-wave signatures and notation for transversely isotropic media: An overview, *Geophysics*, 61(2), 467–483, doi:10.1190/1.1443974.
- Tsvankin, I. (2012), *Seismic Signatures and Analysis of Reflection Data in Anisotropic Media*, third ed., 459 pp., Society of Exploration Geophysicists, Tulsa, Oklahoma, USA.
- White, I. (2016), RCP Sponsors Meeting Report. Spring 2016. The Vaca Muerta Project. Reservoir response to hydraulic fracturing, *Tech. rep.*, Reservoir Characterization Project (RCP), Colorado School of Mines, Golden, Colorado, USA.
- White, J. E. (1983), *Underground Sound: Application of Seismic Waves*, 253 pp., Elsevier.
- Zeller, M., S. B. Reid, G. P. Eberli, R. J. Weger, and J. L. Massafiero (2015), Sequence architecture and heterogeneities of a field - Scale Vaca Muerta analog (Neuquen Basin, Argentina) - From outcrop to synthetic seismic, *Marine and Petroleum Geology*, 66, 829–847, doi:10.1016/j.marpetgeo.2015.07.021.